bioRxiv preprint doi: https://doi.org/10.1101/2021.10.15.464594; this version posted October 18, 2021. The copyright holder for this preprint (which was not certified by peer review) is the author/funder. All rights reserved. No reuse allowed without permission.

Source-sink connectivity: a novel resting-state EEG marker of the epileptogenic zone

Kristin M. Gunnarsdottir[1], Adam Li[+1], Rachel J. Smith[+1], Joon-Yi Kang[2], Nathan E. Crone[2], Anna Korzeniewska[2], Adam Rouse[3], Nathaniel Cameron[3], Iahn Cajigas[4], Sara Inati[5], Kareem A. Zaghloul[5], Varina L. Boerwinkle[6], Sarah Wyckoff[6], Nirav Barot[7], Jorge Gonzalez-Martinez[*7], and Sridevi V. Sarma[*1]

Abstract

Over 15 million epilepsy patients worldwide have medically refractory epilepsy (MRE), i.e., they do not respond to anti-epileptic drugs. Successful surgery is a hopeful alternative for seizure freedom but can only be achieved through complete resection or disconnection of the epileptogenic zone (EZ), the brain region(s) where seizures originate. Unfortunately, surgical success rates vary between 30%-70% because no clinically validated biological markers of the EZ exist. Localizing the EZ has thus become a costly and time- consuming process during which a team of clinicians obtain non-invasive neuroimaging data, which is often followed by invasive monitoring involving days-to-weeks of EEG recordings captured intracranially (iEEG). Clinicians visually inspect iEEG data, looking for abnormal activity (e.g., low-voltage high frequency activity) on individual channels occurring immediately before seizures. They also look for abnormal spikes that occur on iEEG between seizures ("resting-state"). In the end, clinicians use <1% of the iEEG data captured to assist in EZ localization (minutes of seizure data versus days of recordings), missing opportunities to leverage these largely ignored data to better diagnose and treat patients.

Intracranial EEG offers a unique opportunity to observe rich epileptic cortical network dynamics but waiting for seizures to occur increases patient risks associated invasive monitoring. In this study, we aim to leverage iEEG data in between seizures by developing a new networked-based resting-state iEEG marker of the EZ. We hypothesize that when a patient

bioRxiv preprint doi: https://doi.org/10.1101/2021.10.15.464594; this version posted October 18, 2021. The copyright holder for this preprint (which was not certified by peer review) is the author/funder. All rights reserved. No reuse allowed without permission.

is not seizing, it is because the EZ is inhibited by neighboring nodes. We develop an algorithm that identifies two groups of nodes from the resting-state iEEG network: those that are continuously inhibiting a set of neighboring nodes ("sources") and the inhibited nodes themselves ("sinks"). Specifically, patient-specific dynamical network models (DNMs) are estimated from minutes of iEEG and their connectivity properties reveal top sources and sinks in the network, with each node being quantified by a source-sink index (SSI). We validate the SSI index in a retrospective analysis of 65 patients by using the SSI of the annotated EZ as a metric to predict surgical outcomes. SSI predicts with an accuracy of 79%, compared to the accuracy of clinicians being 43% (successful outcomes). In failed outcomes, we identify regions of the brain with high SSIs that were untreated. When compared to high frequency oscillations, the most common resting-state iEEG feature proposed for EZ localization, SSI outperformed in predictive power (by a factor of 1.2) suggesting SSI as a resting-state EEG fingerprint of the EZ.

Author affiliations:

* Co-senior authors

+ Co-second authors

1 Department of Biomedical Engineering, Johns Hopkins University, Baltimore, MD 21218, USA

2 Department of Neurology-Epilepsy, Johns Hopkins School of Medicine, Baltimore, MD 21205, USA

3 Department of Neurosurgery, University of Kansas Medical Center, Kansas City, KS 66160, USA

4 Department of Neurosurgery, University of Miami Miller School of Medicine, Miami, FL 33136, USA

bioRxiv preprint doi: https://doi.org/10.1101/2021.10.15.464594; this version posted October 18, 2021. The copyright holder for this preprint (which was not certified by peer review) is the author/funder. All rights reserved. No reuse allowed without permission.

5 Surgical Neurology Branch, National Institute of Neurological Disorders and Stroke, National Institutes of Health, Bethesda, MD 20892, USA

6 Barrow Neurological Institute, Phoenix Children's Hospital, Phoenix, AZ 85016, USA

7 Department of Neurosurgery, University of Pittsburgh, Pittsburgh, PA 15213, USA

Correspondence to: Author name

Full address

E-mail

Running title: Source-sink index to localize the EZ

Keywords: Epileptogenic zone; Interictal;

Abbreviations: MRE = Medically refractory epilepsy; EZ = epileptogenic zone;

Introduction

Epilepsy is a chronic neurological disorder characterized by unprovoked, recurrent seizures and affects over 60 million people worldwide.[1] Although about 70% of patients diagnosed with epilepsy respond positively to medication, 30% have seizures that cannot be controlled with drugs.[2–4] Patients with medically refractory epilepsy (MRE) commonly experience comorbid illnesses, an increased risk of mortality, lose their independence, and are frequently hospitalized, accounting for 80% of the $16 billion spent annually treating epilepsy patients.[5–11]

The most effective treatments for MRE are interventions that surgically remove or disconnect the epileptogenic zone (EZ), which is defined as the minimal area of brain tissue that is responsible for initiating seizures and whose removal (or disconnection) is necessary for complete seizure-freedom.[12] A successful surgical outcome depends on the type of epilepsy

bioRxiv preprint doi: https://doi.org/10.1101/2021.10.15.464594; this version posted October 18, 2021. The copyright holder for this preprint (which was not certified by peer review) is the author/funder. All rights reserved. No reuse allowed without permission.

and the ability to precisely identify and completely resect the EZ, but current surgical success rates vary significantly, rendering 20-80% of patients seizure free.[13,14]

The objective of resective surgery is the complete removal, inactivation or disconnection of the EZ, with preservation of eloquent cortex. Before surgery, patients undergo a thorough evaluation process to determine the location and extent of the EZ. First, non-invasive methods such as scalp EEG, MRI, PET and SPECT are used to define the location and boundaries of the EZ. If non-invasive methods are discordant or inconclusive in localizing the EZ, invasive monitoring with intracranial EEG (iEEG) is often needed.[15] Following electrode implantation, the patient remains in the hospital for several days to weeks waiting for a sufficient number of seizure (ictal) events because the current clinical standard primarily entails visually analyzing multiple of these events, looking for abnormal epileptic activities, in order to localize the EZ.[16] Specifically, two types of iEEG analyses are performed by highly qualified epileptologists[17]. Ictal (seizure) recordings are inspected to identify various epileptic signatures such as repetitive spikes, rhythmic slow waves or rapid fast intracortical frequencies.[16,18] Based on these findings, a multidisciplinary team of clinicians then form a hypothesis on which electrodes are recording from the EZ. Ictal iEEG data are of higher value for localization purposes, but interictal (between seizure) iEEG data are also inspected to identify abnormal electrographic spikes. The area of cortex that generates interictal spikes is referred to as the irritative zone and channels on which such spikes are observed are denoted as possible EZ nodes.[15] However, it is often difficult to distinguish between propagated and locally generated discharges in iEEG recordings, making interictal spikes an unreliable iEEG marker for the EZ.[16] Thus, the gold standard predominantly relies on inspecting seizure events and as such, more than 99% of the iEEG recordings captured invasively from patients are ignored.

No iEEG markers are currently used in the clinical workflow to specifically assist in the identification of the EZ although many computational approaches have been proposed. In line

bioRxiv preprint doi: https://doi.org/10.1101/2021.10.15.464594; this version posted October 18, 2021. The copyright holder for this preprint (which was not certified by peer review) is the author/funder. All rights reserved. No reuse allowed without permission.

with the standard of care visual analysis, most of the proposed methods depend on seizure data (e.g., [20,24–33]). Nevertheless, using seizure independent (interictal) data has been of high interest as well, as this could significantly speed up the pre-surgical evaluation process. The most frequently proposed interictal marker of the EZ are high frequency oscillations (HFOs).[34,38–42] However, the reliability of HFOs as an iEEG marker of the EZ is debatable[46] and by treating each channel independently, these methods fail to capture network properties of the brain. Additionally, a majority of the aforementioned methods depend on epileptiform signatures being observable in the signals rather than detecting the underlying dynamical properties of the epileptic network.

In this study, we aim to leverage data captured between seizures to localize the EZ. We hypothesize that when a patient is not having a seizure, it is because the EZ is being inhibited by neighboring regions. We then develop and test a new interictal iEEG marker of the EZ by identifying two groups of network nodes from a patient's interictal iEEG network: those that are continuously inhibiting a set of their neighboring nodes (denoted as “sources”) and the inhibited nodes themselves (denoted as “sinks”). Specifically, we develop a computational tool that i) estimates patient-specific dynamical network models from interictal iEEG data and ii) uses source-sink connectivity properties of the models to identify pathological nodes (iEEG channels) in the network that correspond to the EZ. We apply our algorithm to interictal iEEG snapshots from 65 patients treated across 6 clinical centers and evaluate performance by i) comparing the EZ channels identified by our algorithm to those identified by clinicians and ii) predicting surgical outcomes as a function of source-sink features by employing the random forest framework.

bioRxiv preprint doi: https://doi.org/10.1101/2021.10.15.464594; this version posted October 18, 2021. The copyright holder for this preprint (which was not certified by peer review) is the author/funder. All rights reserved. No reuse allowed without permission.

Materials and methods

Patient population

Sixty-five adults (mean age 33.5 $\pm$ 13.0 (mean$\pm$s.d.) years) with medically refractory epilepsy who underwent intracranial EEG monitoring with stereotactic depth (SEEG) electrodes and received subsequent treatment were selected for the study. Treatment options include resective surgery (39 patients), laser ablation (17 patients) or responsive neurostimulation (RNS, 9 patients). Patients were treated at one of the following institutions: Cleveland Clinic (CC), Johns Hopkins Hospital (JHH), University of Kansas Medical Center (KUMC), University of Miami Hospital (UMH), National Institutes of Health (NIH) or University of Pittsburgh Medical Center (UPMC). All patients had a minimum of one year follow-up subsequent to their last treatment procedure to determine treatment outcomes. Patients who had a follow-up period of less than one year and patients who did not receive treatment following presurgical evaluation (e.g., due to non-localizable EZ or EZ located in eloquent cortex) were excluded from the study. Patient population statistics are summarized in Table 1. The study was approved by the Institutional Review Board (IRB) at each clinical institution; Cleveland Clinic's IRB, Johns Hopkins Medicine IRB, University of Kansas Human Research Protection Program, University of Miami Human Subject Research Office, National Institutes of Health IRB, and the University of Pittsburgh IRB. All clinical decisions were made independent of this study.

bioRxiv preprint doi: https://doi.org/10.1101/2021.10.15.464594; this version posted October 18, 2021. The copyright holder for this preprint (which was not certified by peer review) is the author/funder. All rights reserved. No reuse allowed without permission.

Data collection

SEEG recordings

The SEEG data were recorded using either a Nihon Kohden (Nihon Kohden America, Foothill Ranch, CA, USA) or Natus (Natus Medical Inc., Pleasanton, CA, USA) diagnostic and monitoring system at a typical sampling frequency of 1 or 2 kHz. A small subset of recordings was recorded at a sampling frequency of 500/512 Hz. The placement of each electrode was determined by the clinical team at each center based on patient history and available non-invasive data. For each patient, a minimum of 20 seconds and a maximum of 16 minutes of interictal snapshots (average duration 5.3 ± 4.2 minutes) were randomly selected for analysis. Interictal periods were recorded at least one hour away from seizure events and no specific selection criteria (such as the presence or absence of epileptiform activity) were applied.

Clinical annotations of the EZ

At each epilepsy center, an EZ hypothesis was formulated by the clinical team based on the comprehensive patient data (non-invasive and invasive) gathered throughout the presurgical evaluation procedure independent of this study. Epileptologists describe the anatomical location and extent of the EZ by means of visual analysis of the invasive data by identifying the regions involved at seizure onset. The clinically annotated EZ (CA-EZ) is defined as the anatomical areas to be treated (resected, ablated or stimulated) to permanently extinguish the epileptiform activity, and includes SEEG channels demonstrating the earliest electrophysiological changes (generally characterized by low voltage fast activity) at the beginning of an ictal event, as well as channels involved in early propagation of the seizure activity.

bioRxiv preprint doi: https://doi.org/10.1101/2021.10.15.464594; this version posted October 18, 2021. The copyright holder for this preprint (which was not certified by peer review) is the author/funder. All rights reserved. No reuse allowed without permission.

Clinical classification of surgical outcomes

Post-surgical clinical outcomes were classified by the clinical experts at each center according to the Engel Surgical Outcome Scale[47] and the International League Against Epilepsy (ILAE) classification system.[48] Successful surgical outcomes were defined as seizure free (Engel class I and ILAE scores 1-2) and failure outcomes as seizure recurrence (Engel classes II-IV and ILAE scores 3-6) at 12+ month post operation. Out of the 65 patients in the dataset, 28 patients had a successful surgical outcome whereas 37 patients experienced seizures after receiving treatment (failed outcome). Previous outcome studies have shown that patients with visible lesions on MRI have higher success rates as seizures likely originate from the lesion or its vicinity thus making the EZ better localizable.[49] In contrast, non-lesional patients, and patients with extra-temporal or multi-focal epilepsy are at a higher risk for poor surgical outcomes.[18,50–52] To better define the clinical complexity of each patient, the clinical team assigned patients to three additional categories as follows: 1) lesional (visible lesions on MRI) or non-lesional, 2) mesial temporal or extra-temporal, and 3) focal or multi-focal.

Data pre-processing

The data were bandpass filtered between 0.5 and 300 Hz with a fourth order Butterworth filter, and notch filtered at 60 Hz with a stopband of 2 Hz. A common average reference was applied to remove common noise from the signals. Finally, SEEG channels not recording from grey matter or otherwise deemed "bad" (e.g., broken or excessively noisy or artifactual) by visual inspection were discarded from each patient's dataset. The continuous SEEG recordings were divided into non-overlapping 500-msec windows for modeling and feature extraction (see details below). All data processing and analysis were performed using MATLAB R2020b (MathWorks, Natick, MA). Models for predicting surgical outcomes were built using Python3.6 (Python Software Foundation, Wilmington, DE).

bioRxiv preprint doi: https://doi.org/10.1101/2021.10.15.464594; this version posted October 18, 2021. The copyright holder for this preprint (which was not certified by peer review) is the author/funder. All rights reserved. No reuse allowed without permission.

Sources and sinks in the epileptic brain network

In contrast to the clinical gold standard which primarily involves a visual inspection of seizure events to localize the EZ, we performed our analysis exclusively on interictal, seizure-free data. This leads to a fundamental question: *how can one identify where seizures start in the brain without ever observing a seizure?* Our source-sink hypothesis states that seizures are suppressed because epileptogenic regions (denoted as sinks) are persistently being inhibited by neighboring regions (denoted as sources). The concepts of sources and sinks within a network is well established and has been applied to many analyses of network systems.[53] In our application a "sink" node is a region in the brain network that is being highly influenced by other nodes but is not influential itself. In contrast, a "source" node is a region that is highly influential to other nodes but is not being influenced by other nodes. During rest, our conjecture is that the onset of seizure is prevented by a strong inhibition exerted on the EZ by its neighboring brain regions, which restricts the discharge and propagation of the seizure activity, i.e., EZ regions are sinks that cannot influence the rest of the network. When an epilepsy patient has a seizure however, the EZ is triggered and the EZ nodes transition into sources as they work together as a collective group to initiate and spread seizure activity. Fig. 1 shows a schematic representation of the source-sink hypothesis.

bioRxiv preprint doi: https://doi.org/10.1101/2021.10.15.464594; this version posted October 18, 2021. The copyright holder for this preprint (which was not certified by peer review) is the author/funder. All rights reserved. No reuse allowed without permission.

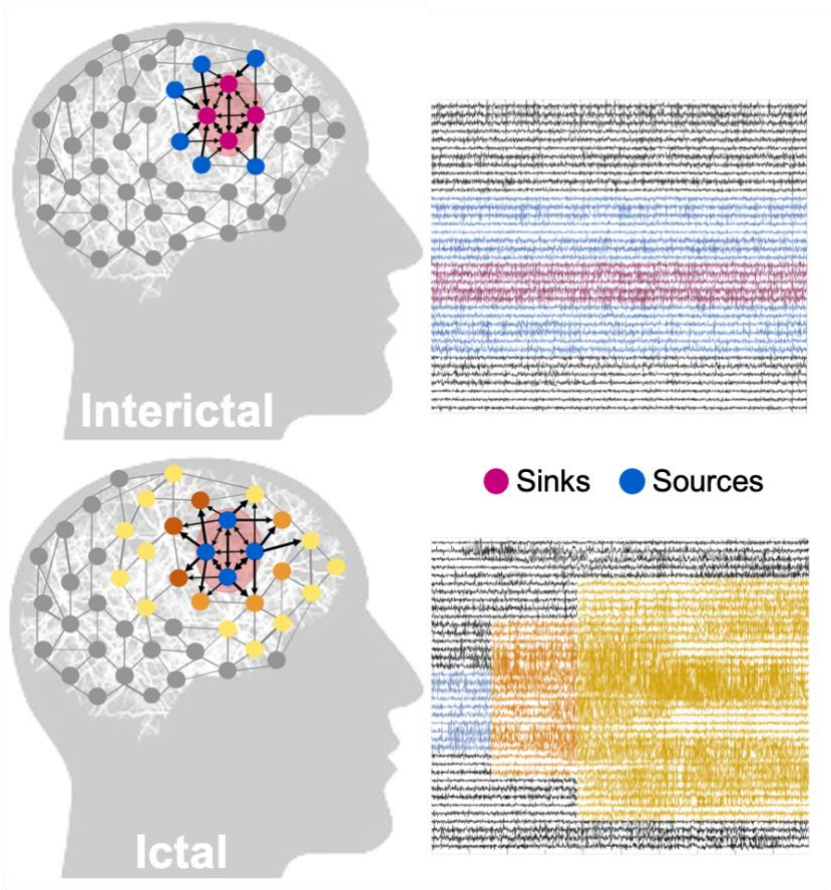

Figure 1. Source-sink hypothesis. Top: During interictal periods, epileptogenic nodes (shaded red region) are sinks that are strongly inhibited (influenced) by neighboring regions (sources) to prevent seizures. Bottom: During ictal (seizure) periods however, epileptogenic nodes become sources as they work together as a tightly coupled group to initiate and spread epileptogenic activity to other regions of the brain.

Clinical evidence supporting the source-sink hypothesis

From a cytological perspective, the source-sink hypothesis is supported by evidence that seizures are prevented when the EZ is effectively inhibited by other brain regions. Glutamate, the primary excitatory neurotransmitter in the brain, has been implicated as a neurotoxic agent in epilepsy. A healthy brain function requires a balance between glutamate uptake and release to maintain the concentration of extracellular glutamate within a homeostatic range.[54] Several studies have demonstrated the existence of elevated levels of extracellular glutamate in animal models of epilepsy[55] and human patients.[56] In addition, the presence of sodium dependent

bioRxiv preprint doi: https://doi.org/10.1101/2021.10.15.464594; this version posted October 18, 2021. The copyright holder for this preprint (which was not certified by peer review) is the author/funder. All rights reserved. No reuse allowed without permission.

glutamate transporters (GLTs) is thought to be crucial to prevent accumulation of neurotoxic levels of glutamate in the extracellular space by clearing unbound extracellular glutamate. Findings suggest that fluctuations in the expression of such GLTs may play a role in the expression of epileptogenicity.[57] In fact, previous studies have shown an increased number of GLTs in human dysplastic neurons and posit that it enables a "protective" inhibitory mechanism surrounding the epileptogenic cortex.[58] Taking this evidence together, the inhibitory (the sink phenomena) and the excitatory (the source phenomena) events within the potential EZ have its biological substrate in the differential expression of glutamate transporters within the EZ.

iEEG studies supporting the source-sink hypothesis

iEEG studies also provide evidence that support our source-sink hypothesis. Several studies have demonstrated a high inward directed influence to the EZ at rest.[59–61] In a recent study by Narasimhan et al.[59] the authors state that high inward connectivity may reflect inhibitory input from other regions to prevent the onset and spread of seizure activity, but the direction of these signals may flip when seizure activity begins. This conjecture is further supported by iEEG studies in neocortical epilepsy demonstrating functional isolation of epileptogenic areas at rest[62] and that increased synchronization in seizure-onset regions may be suggestive of an inhibitory surround.[63] It has also been hypothesized that widespread network inhibition seen in temporal lobe epilepsy may have evolved to prevent seizure propagation[63] and that a reduction of the inhibitory influence may lead to increased excitability and propagation of seizure activity.[64]

In this study, we formalize the above evidence and build dynamical network models (DNMs) of the interictal iEEG activity to identify sources and sinks of the network from DNM

bioRxiv preprint doi: https://doi.org/10.1101/2021.10.15.464594; this version posted October 18, 2021. The copyright holder for this preprint (which was not certified by peer review) is the author/funder. All rights reserved. No reuse allowed without permission.

connectivity parameters. Source-sink indices are computed for each network node (see below) which are then used to predict treatment outcomes.

Dynamical network models

The DNMs are generative models that characterize how each iEEG channel dynamically influences the rest of the network. The interictal DNM takes the form of a linear time-varying (LTV) model that mathematically describes how each observed brain region (i.e., iEEG channel signal) interacts with other regions. The LTV DNM is composed of a sequence of linear time invariant (LTI) DNMs derived from smaller windows of the data. Each LTI model takes the following form:

$$\boldsymbol{x}(t+1) = \boldsymbol{A}\boldsymbol{x}(t) \quad (1)$$

Where $\boldsymbol{x}(t)\epsilon\mathbb{R}^N$ is the state vector and represents the implanted iEEG channels, $\boldsymbol{A}\epsilon\mathbb{R}^{NxN}$ is the state transition matrix, which describes how the iEEG channels interact and how their activity evolves over time, and N is the number of iEEG channels. In our previous work, we showed how DNMs can be derived using least squares estimation and how they accurately reconstruct the iEEG data (see Supplementary Fig. 1 for an example of actual versus simulated iEEG data).[65] Importantly, systems theory can be employed to uncover the dynamics and properties of the DNMs which we will use to ultimately assist in accurately localizing the EZ. In these models, element $\boldsymbol{A}_{ij}$ describes how the *present* activity of channel i influences the *future* activity of channel j. More generally, the i-th row of $\boldsymbol{A}$ dictates the iEEG network's cumulative functional effect on node i, while the j-th column determines the functional effect that the activity of node j exerts on the entire network. We note that due to the resolution of the iEEG recordings, the DNMs cannot distinguish between excitatory and inhibitory connections in the network. Instead, we simply quantify the amount of "influence" one node has on another.

bioRxiv preprint doi: https://doi.org/10.1101/2021.10.15.464594; this version posted October 18, 2021. The copyright holder for this preprint (which was not certified by peer review) is the author/funder. All rights reserved. No reuse allowed without permission.

Identifying sources and sinks in the iEEG DNM

We define two special groups of nodes in the iEEG DNM, subject to the source-sink hypothesis. *Source* nodes (blue nodes in Fig. 2A) are nodes that generally have high values (in magnitude) in their columns of the $\boldsymbol{A}$ matrix (high influence *on* others) but low values across their rows (low influence *from* others). In contrast, *sinks* (pink nodes in Fig. 2A) exhibit the opposite pattern, high row values and low column values.

Computing dynamic and constant source-sink indices

Source-sink 2D-space: To identify the top sources and sinks in each patient's DNM, we quantified each channel's source-sink characteristics by computing the amount of influence to and from the channel based on the sum of the absolute values (also known as the 1-norm) across its row and column in $\boldsymbol{A}$ (Fig. 2C), respectively. Once we obtained the total influence to/from each channel, we placed the channels in the source-sink 2D-space (SS-space, Fig. 2D) in order to compute a source-sink index (SSI) for each channel. When drawn in the SS-space, sources are channels located at the top left (blue circles), whereas sinks (pink circles) are located at the bottom right.

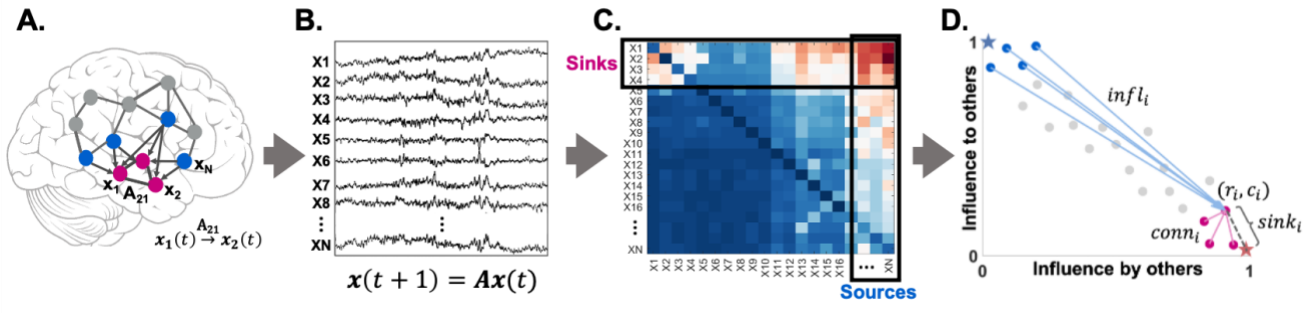

Figure 2. A. A N-channel iEEG network example. B. Signals obtained from the implanted iEEG channels. C. Corresponding $\boldsymbol{A}$ matrix, estimated from the signals in B. D. 2D source-sink representation of the iEEG network with sink index ($sink_i$), source influence ($source_i$) and sink connectivity ($conn_i$) labeled.

bioRxiv preprint doi: https://doi.org/10.1101/2021.10.15.464594; this version posted October 18, 2021. The copyright holder for this preprint (which was not certified by peer review) is the author/funder. All rights reserved. No reuse allowed without permission.

Next, we computed SSI for each channel. The SSI is a product of three metrics subject to the source-sink hypothesis:

Sink Index: The first criterion from our source-sink hypothesis requires an iEEG channel to be a top sink in the iEEG network to be considered an EZ channel. The sink index captures how close channel i is to the ideal sink (see Fig. 2D, pink star). The larger the sink index, the more likely the channel is a sink.

Source Influence: The second criterion requires an EZ channel to be highly influenced by the top sources of the iEEG network. The source influence index quantifies how much the top sources influence channel i. A high source influence suggests that channel i receives strong influence from the top sources in the interictal DNM.

Sink Connectivity: The third and final criterion from our source-sink hypothesis for a node to be considered an EZ node is that it is highly connected to other sinks so that it can collaborate to generate a seizure. The sink connectivity index quantifies the strength of connections from the top sinks to channel i, and thus, the higher the sink connectivity, the stronger influence channel i receives from the top sinks in the network.

Source-sink index (SSI): Finally, a source-sink activation index was computed for each iEEG channel in each window as the product of sink index, source influence and sink connectivity. In line with the source-sink hypothesis stated above, the SSI is high if all three indices are high. Therefore, we expect EZ nodes to have a high SSI and non-EZ nodes to have a lower SSI during interictal periods.

Unlike seizure activity, interictal activity is relatively stable, with little deviation from a baseline value over time. As a result, there is little variation in the sequence of $\boldsymbol{A}_w$ matrices and consequently in the source-sink behavior of individual channels across windows during interictal periods. Thus, we also computed a constant, average $\boldsymbol{A}$ matrix to represent each

bioRxiv preprint doi: https://doi.org/10.1101/2021.10.15.464594; this version posted October 18, 2021. The copyright holder for this preprint (which was not certified by peer review) is the author/funder. All rights reserved. No reuse allowed without permission.

patient's interictal DNM and used it to compute a set of constant source-sink indices for each patient. We refer the reader to Supplementary Methods, section 1.2 for further details of the analysis.

Predicting surgical outcomes using source-sink indices

To evaluate the source-sink indices as interictal iEEG markers of the EZ, we tested their efficacy in predicting surgical outcomes following the same procedure as Li et al[24] (see Supplementary Fig. 2 for a schematic of the experimental design) and compared performance against that of clinicians as well as HFOs, the most common interictal iEEG marker of the EZ. Specifically, we modeled the probability of a successful surgical outcome, p_s, as a function of the three SSI metrics (sink index, source influence and sink connectivity) using a random forest (RF) classifier. We computed the distribution of constant feature values in two sets of channels: i) the CA-EZ and ii) all other channels not labeled as CA-EZ (CA-NEZ). Feature distributions of each set were summarized with the mean and standard deviation, resulting in 12 possible features presented to the RF classifier. Next, we performed a tenfold nested cross-validation (CV), considering a set of hyperparameters, and performed statistical analysis (described below) on the final classification performance to determine the most robust feature representation.

Predicting surgical outcomes using HFOs

We compared the predictive value of the source-sink indices to that of HFOs,[66,67] which have been actively explored as interictal biomarkers of the EZ. We detected HFOs in the interictal data segments using the root-mean-square detector developed by Staba et al[68] (see Supplementary Methods, section 1.4 for details).

bioRxiv preprint doi: https://doi.org/10.1101/2021.10.15.464594; this version posted October 18, 2021. The copyright holder for this preprint (which was not certified by peer review) is the author/funder. All rights reserved. No reuse allowed without permission.

HFO rate (number of HFOs per minute per channel) is amongst the most commonly used metrics to test the value of HFOs as a biomarker of the EZ (e.g., [38,42,45,61,68–72] to name a few). Thus, we chose to compare the performance of the source-sink indices to that of HFO rate by modeling p_s as a function of HFO rate following the exact same paradigm as for the source-sink indices described above.

Clinical annotations of CA-EZ and SSI correspondence

To further evaluate the source-sink index as an iEEG marker of the EZ, the clinical team at each center reviewed the source-sink results for each patient and ranked the clinical correspondence between the CA-EZ and the nodes that have high SSIs. Specifically, for each patient, clinicians at the corresponding center were presented with a SS-space (Fig. 2D), which showed the location of each implanted iEEG channel in the source-sink space, as well as the strongest connections from the top sources and sinks and where they point to. The clinical team then compared the source-sink results to the clinically annotated EZ regions and rated the clinical correspondence between the two sets as either: 1) *agreement*, defined as a) *strong agreement* if there was as a significant overlap with the clinically annotated EZ or b) *some agreement* if there was some overlap with the CA-EZ regions or the channels with the highest SSI were within the same functional network as the CA-EZ , or 2) *no agreement,* defined as no overlap with CA-EZ regions.

Statistical analysis

Each RF model (source-sink and HFO) was validated using a tenfold CV. In order to control against overfitting of the models, we used a nested CV scheme, where we split the dataset into a training, validation and a held-out test dataset.[24] In each such split, the hyperparameters were tuned using the training and validation data (70% of the dataset), and performance was then

bioRxiv preprint doi: https://doi.org/10.1101/2021.10.15.464594; this version posted October 18, 2021. The copyright holder for this preprint (which was not certified by peer review) is the author/funder. All rights reserved. No reuse allowed without permission.

evaluated on the test dataset by applying a varying threshold to the model's output and computing a receiver operating characteristic (ROC) curve, which plots true positive rates against false positive rates for various threshold values. We then selected the threshold that maximized prediction accuracy in each split and evaluated performance by comparing each patient's predicted outcome to the actual outcome.

We used five metrics to measure model performance: i) area under the curve (AUC) of the ROC, ii) prediction accuracy iii) precision, iv) sensitivity, and v) specificity (see metric definitions in Supplementary section 1.6). We report results of the ten CV folds (mean $\pm$ s.d.) below. Finally, we compared the performance metrics of the source-sink indices to those of HFO rates using a paired two-sample t-test. In all t-tests performed, the null hypothesis was that the two distributions have equal means and the alternate hypothesis was that the means are different. Lastly, outcome predictions of the two models were compared using a McNemar's test for paired nominal data. For all tests, a p-value ≤ 0.05 was considered to be statistically significant.

Data availability

We released the raw iEEG data for patients from XX, XX, and XX in the OpenNeuro repository in the form of BIDS-iEEG (insert link here). Due to restrictions on data sharing from CC, we were unable to release the iEEG data that we received from this site. Dataset from CC is available upon request from authors at the CC.

bioRxiv preprint doi: https://doi.org/10.1101/2021.10.15.464594; this version posted October 18, 2021. The copyright holder for this preprint (which was not certified by peer review) is the author/funder. All rights reserved. No reuse allowed without permission.

Results

The source-sink index highlights CA-EZ regions in patients with successful outcomes

From each patient's interictal DNM, we quantified source-sink characteristics of every iEEG channel by computing its dynamic SSI in every 500-msec sliding-window of the interictal recording (see Fig. 3A for examples of 1-minute snapshot of iEEG data and the corresponding spatiotemporal SSI heatmaps for three patients with different surgical outcomes). Fig. 3B shows the constant interictal SSI of each iEEG contact, overlaid on each patient's implantation map and the placement of each channel in the 2D source-sink space is shown in Fig. 3C.

A high SSI indicates that the channel is a top sink that is both highly connected to other sinks and strongly influenced by the top sources of the network. In patient 1, the iEEG channels with the highest SSI match the channels identified as the EZ by clinicians (three out of three). In this patient, all three CA-EZ channels were included in the surgical treatment (laser ablation) which led to a complete seizure freedom. In patient 2 however, only two out of thirteen CA-EZ regions have high SSI values whereas the other iEEG channels with high values were not a part of the CA-EZ and thus were not treated during surgery. This patient did not become seizure free post-treatment. Finally, patient 3 demonstrates an interesting case. This patient had two surgeries; first a laser ablation of superior frontal and cingulate gyri (contacts on L' and G' electrodes) which resulted in seizure recurrence, and later a resection of pre- and post-central as well as supplementary motor areas (M' electrode) which led to a complete seizure freedom. Interestingly, when the iEEG channels first identified as CA-EZ (CA-EZ_1) are considered, none of these channels are amongst the top 10% of channels with highest SSI.

bioRxiv preprint doi: https://doi.org/10.1101/2021.10.15.464594; this version posted October 18, 2021. The copyright holder for this preprint (which was not certified by peer review) is the author/funder. All rights reserved. No reuse allowed without permission.

However, the majority of the channels with highest SSI correspond to the second identified CA-EZ (CA-EZ_2; M' electrode) that ultimately led to a successful outcome in this patient.

Identifying channels with highest SSI

As Fig. 3A shows, the source-sink metrics remain consistent with little variation of the SSI of each channel across the interictal recordings, Thus, we computed a constant $\boldsymbol{A}$ matrix to represent each patient's interictal DNM. From this matrix, we identified the top sources and sinks in the iEEG network by computing the total influence to and from each channel and placing the channels in the 2D source-sink space (see Fig. 3C for three patient examples) based on their total influence. In patients with successful surgical outcomes, the CA-EZ channels are expected to be a subset of the top sinks (Fig. 3C, top). The blue and pink arrows indicate the strongest connections from the top sources and sinks, respectively, and the channels they point to. The most likely candidates of the true EZ, based on the source-sink hypothesis, were the subset of top sinks that were highly connected to other sinks and strongly influenced by top sources. In general, the top sources and sinks point to the CA-EZ channels in success patients (Fig. 3C, top), whereas they may also connect to other channels in patients with failed surgical outcomes (Fig. 3C, middle). In patient 3 (Fig. 3C, bottom), who continued to have seizures after the first surgery (failed outcome), the CA-EZ_1 are not amongst the top sinks in the iEEG network, whereas the majority of CA-EZ_2, the set of channels that led to seizure-freedom post-surgery, are top sinks. In addition, the latter set of channels are highly influenced by the top sources and sinks in the network and thus are considered likely candidates of the true EZ by the source-sink algorithm.

bioRxiv preprint doi: https://doi.org/10.1101/2021.10.15.464594; this version posted October 18, 2021. The copyright holder for this preprint (which was not certified by peer review) is the author/funder. All rights reserved. No reuse allowed without permission.

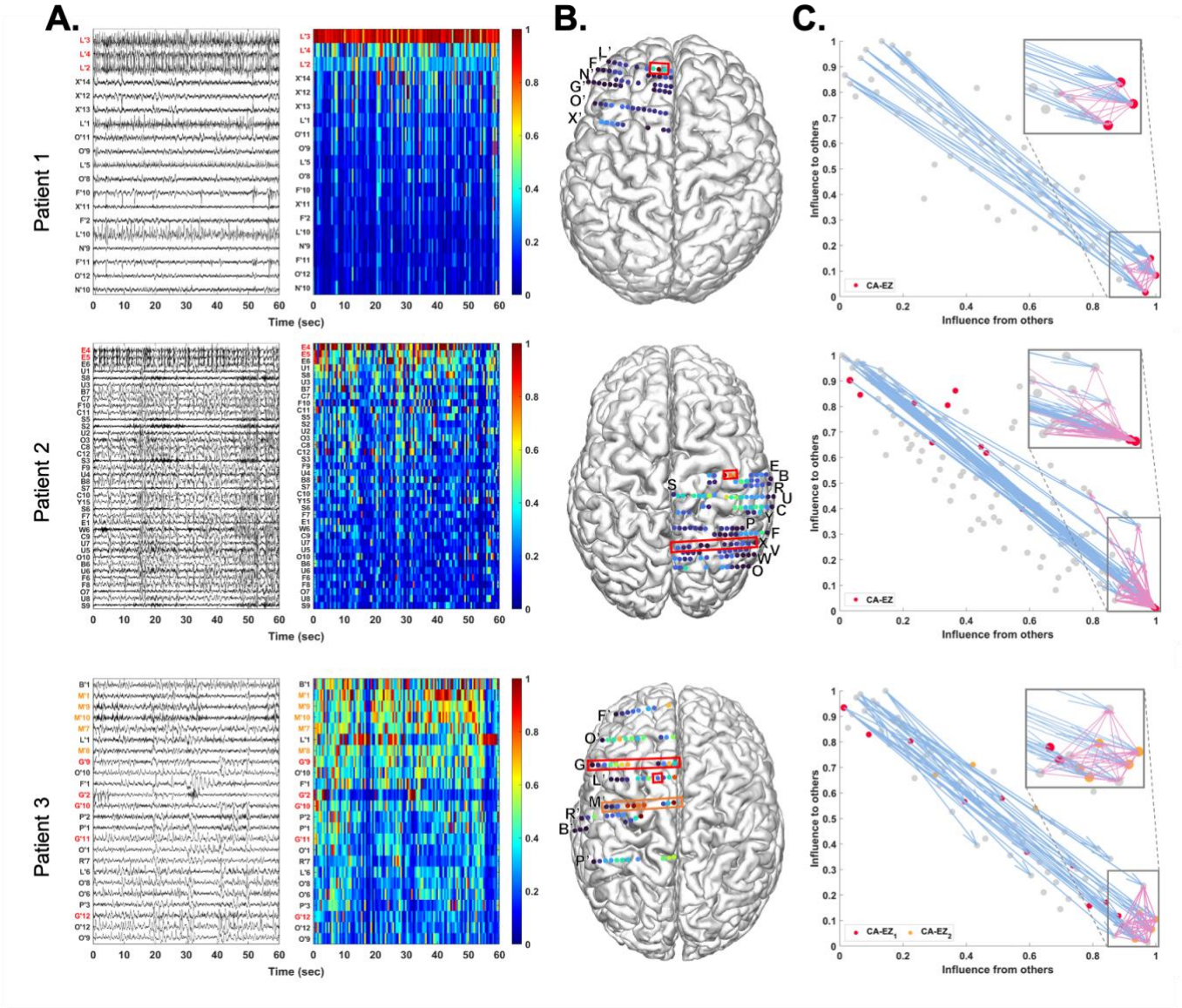

Figure 3. Three patient examples; Patient 1 (top) had a successful surgical outcome. Patient 2 (middle) had a failed surgical outcome. Patient 3 (bottom) had two surgeries. After the first surgery, the patient continued to have seizures (failed outcome) but became seizure free (successful outcome) after the second surgery. A. A 1-minute interictal iEEG snapshot (left) and the resulting SSI of every channel (right). Channels are arranged from highest to lowest stationary interictal SSI. CA-EZ channels are colored red. For patient 3, the CA-EZ from the second surgery are colored orange. Only the top 30% of channels are shown for better visualization purposes, and all channels not shown have low SSI values. In the success patient (top), CA-EZ channels have the highest SSIs, whereas only 2 out of 13 CA-EZ channels have a high SSI in the failure patient (middle). In patient 3 (bottom), the CA-EZ that rendered the patient seizure free has the highest SSIs. B. Stationary SSI of each channel overlaid on the patients' implantation maps. Red/orange boxes outline CA-EZ channels. C. 2D source-sink space. Top sources are located in the top left and top sinks in the bottom right. CA-EZ channels are colored red. The second CA-EZ in patient 3 is colored orange in the bottom panel. The most influential connections from sources (blue arrows) point to the sinks and the strongest connections from sinks (pink arrows) point to other sinks in patient 1 (top), whereas the top sources point to nodes other than top sinks in the failure patient (middle). Top sinks also point to these other nodes.

bioRxiv preprint doi: https://doi.org/10.1101/2021.10.15.464594; this version posted October 18, 2021. The copyright holder for this preprint (which was not certified by peer review) is the author/funder. All rights reserved. No reuse allowed without permission.

Temporal stability of sources and sinks during interictal periods

To verify the stationarity of the SSI over time, we test the sensitivity of the source-sink analysis to duration and timing of the interictal snapshot. Specifically, we computed how many of the top 10% channels with highest constant source-sink indices were captured in windows of five different durations, $ws = \{1, 2, 3, 5, 10\}$ minutes, and compared to how many channels were captured by chance (see further methodological details in Supplementary section 1.3). As Fig. 4 shows, over 90% of the top channels were captured on average for all indices – independent of the timing or duration of the interictal snapshot – compared to a much fewer channels (around 10%) captured by chance ($p \ll 0.05$ for all metrics). This suggests that given any snapshot of interictal data, even as short as 1 minute, the results would be highly comparable to those obtained from the entire interictal snapshot for each patient.

bioRxiv preprint doi: https://doi.org/10.1101/2021.10.15.464594; this version posted October 18, 2021. The copyright holder for this preprint (which was not certified by peer review) is the author/funder. All rights reserved. No reuse allowed without permission.

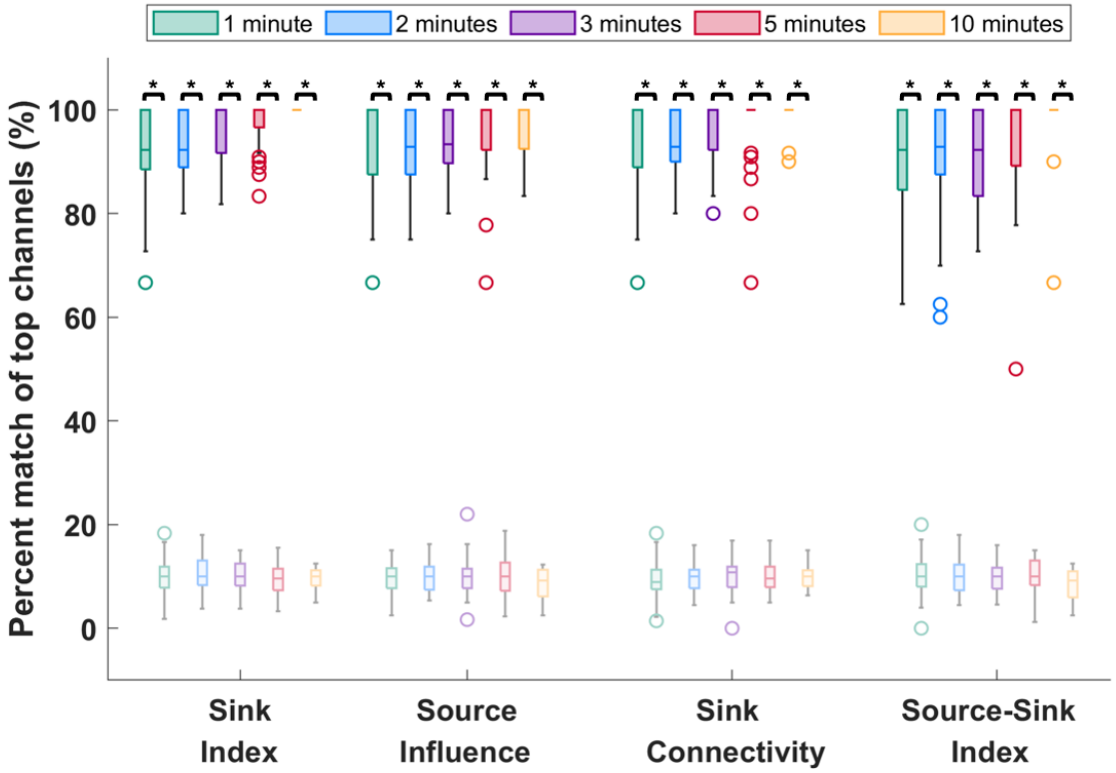

Figure 4. Temporal stability of source-sink indices. Darker colors represent distributions of source-sink indices whereas lighter (transparent) colors represent channels captured by chance. On average, over 90% of channels are captured for all indices, independent of timing or duration of the interictal snapshot selected. Increasing the window size does not change the percentage of captured top channels significantly. In comparison, only around 10% of top channels are captured by chance. The asterisks indicate a statistically significant difference.

Source-sink metrics outperform HFOs in predicting surgical outcomes

As stated above, the SSI, and consequently the three metrics (sink index, source influence and sink connectivity) used to compute the SSI, are significantly higher in CA-EZ channels compared to the rest of the iEEG network in patients with successful surgical outcomes but not necessarily in failure patients ($p_{\mathrm{SSI}}^{success} = 8.26 \times 10^{-7}$ and $p_{\mathrm{SSI}}^{failure} = 0.151$, see other p-values in Supplementary Table 1). Taking advantage of this assumption, we built a RF model to predict the probability of a successful surgical outcome for each patient using i) the source-

bioRxiv preprint doi: https://doi.org/10.1101/2021.10.15.464594; this version posted October 18, 2021. The copyright holder for this preprint (which was not certified by peer review) is the author/funder. All rights reserved. No reuse allowed without permission.

sink metrics and ii) HFO rate, for comparison. The resulting test-set ROC curves are shown in Supplementary Fig. 2. Figs. 7A and B show the predicted probabilities of success (p_s) across all CV-folds, using the source-sink and the HFO model, respectively. The dots are color-coded based on each patient's surgical outcome. A decision threshold of $\alpha = 0.5$ was applied to the estimated probabilities to predict each patient's outcome. Using the source-sink indices (Fig. 7A), the majority of success patients are above the threshold, with $p_s > 0.5$ whereas most failure patients are below it. In contrast, there was not a clear separation between success and failure patients using HFO rate (Fig. 7B).

Fig. 7C compares the performance of the source-sink metrics and HFOs in predicting surgical outcomes. The source-sink metrics outperformed HFO rate with significantly higher AUC, accuracy, average precision and sensitivity ($p_{AUC} = 0.0096, p_{accuracy} = 0.0442, p_{precision} = 0.0023$ and $p_{sensitivity} = 2.03 \times 10^{-4}$). Although the source-sink index had a higher specificity on average, both models performed similarly ($p_{specificity} = 0.7846$). Note that HFO rate was computed across the entire interictal snapshot provided for each patient. The longer the snapshot, the more likely it is to capture HFOs. In contrast, although the source-sink metrics were also computed by averaging across the same recordings for each patient, we showed above that the results remain consistent independent of both timing and length of the recording.

bioRxiv preprint doi: https://doi.org/10.1101/2021.10.15.464594; this version posted October 18, 2021. The copyright holder for this preprint (which was not certified by peer review) is the author/funder. All rights reserved. No reuse allowed without permission.

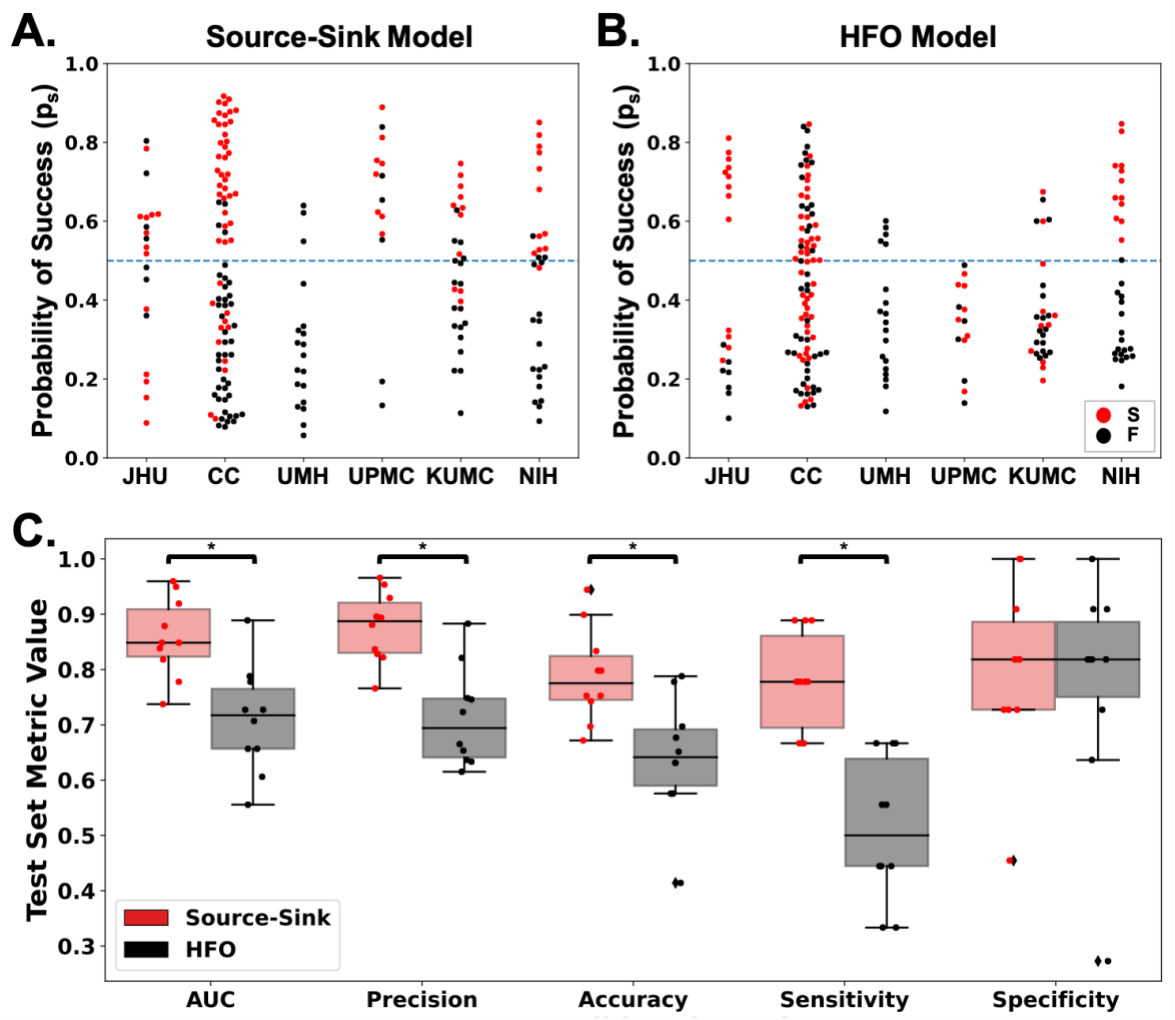

Figure 5. A. Predicted probability of success (p_s) by the source-sink model across all CV folds. Each dot represents one patient and dots are colorcoded by surgical outcome. S=success, F=failure. The dashed blue line represents the decision threshold applied to p_s to predict outcomes. For the source-sink model, the majority of success patients (red dots) have p_s values above the threshold whereas failure patients (black dots) generally have p_s values below the threshold. B. Predicted probability of success p_s) by the HFO model across all CV folds. For the HFO model, there is not as clear separation between the success and failure patients, with both groups having p_s above and below the decision threshold, thus resulting in a lower prediction accuracy. C. Performance comparison of the source-sink metrics (red) to HFO rate (black). Boxes show distributions of each metric across the 10 CV folds. The asterisks indicate a statistically significant difference. The source-sink metrics outperformed HFO rate with significantly higher AUC, accuracy, average precision and sensitivity ($p_{AUC} = 0.0096$, $p_{accuracy} = 0.0442$, $p_{precision} = 0.0023$ and $p_{sensitivity} = 2.03 \times 10^{-4}$) whereas both models had a comparable specificity ($p_{specificity} = 0.7846$). The source-sink metrics had an AUC of 0.86 ± 0.07 compared to an AUC of 0.71 ± 0.10 using HFO rate. The source-sink model also outperformed HFOs in terms of average precision, which weighs the predictive power in terms of the total number of patients, with an average precision of 0.88 ± 0.06 compared to 0.71 ± 0.09 for the HFO rate. Using the source-sink indices, a threshold of $\alpha = 0.5$ applied to p_s for each subject rendered a test-set accuracy of $79.0 \pm 9.1\%$, compared to a considerably lower accuracy of $65.5 \pm 11.4\%$ using HFOs and an even lower clinical success rate of 43% in this dataset. The biggest performance difference between the two models was in terms of sensitivity (true positive rate) where the source-sink model outperformed HFO rate by more than 50% with a sensitivity of 0.78 ± 0.09. However, both models performed similarly in predicting failed outcomes correctly, where the source-sink model had a slightly higher specificity of 0.80 ± 0.16 compared to 0.77 ± 0.20 for the HFOs.

bioRxiv preprint doi: https://doi.org/10.1101/2021.10.15.464594; this version posted October 18, 2021. The copyright holder for this preprint (which was not certified by peer review) is the author/funder. All rights reserved. No reuse allowed without permission.

Source-sink metrics are correlated with treatment outcomes

The separation between the p_s distributions of success versus failure patients is greater for the source-sink model compared to the model using HFO rate, and consequently so is the model's ability to discriminate between the two outcome possibilities ($p = 0.007$). Fig. 6 compares the predicted probability of success on the test set in success versus failure patients of the source-sink metrics (red) and HFOs (black). Each box represents the distribution of p_s values across all CV folds. When further broken down by Engel class (Fig. 6**Error! Reference source not found.**B) or ILAE score (Fig. 6C), we observed a decreasing trend of p_s as the outcome score (and thus also the severity of post-operative seizure outcome) increased using the source-sink metrics. In contrast we did not see this clear separation of p_s values using the HFO model, which had a much greater overlap between classes.

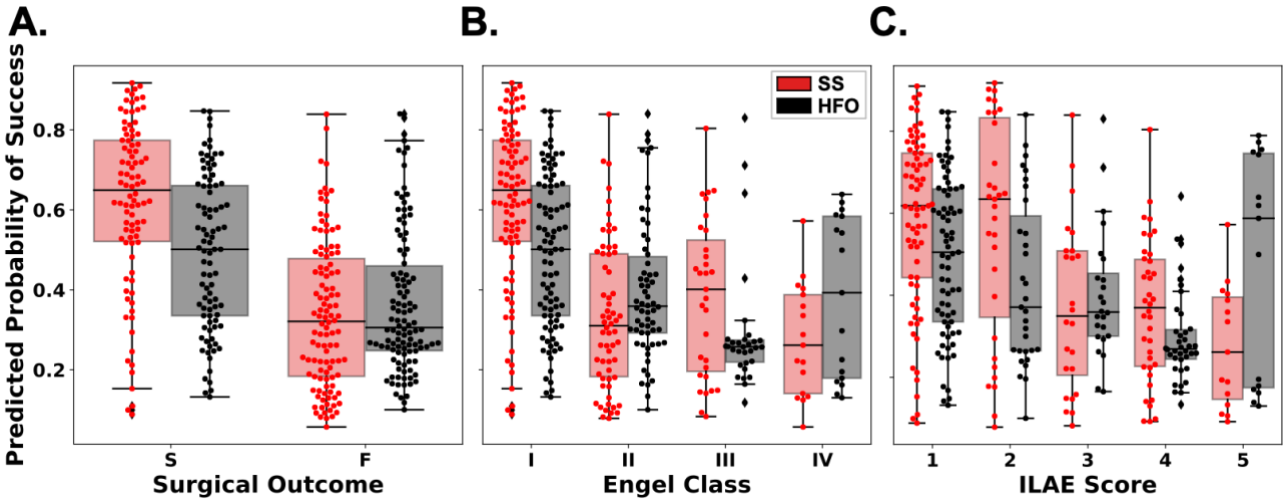

Figure 6. A. Distributions of p_s as predicted by the source-sink model (red) and HFO model (black). There is a clear separation of the distributions for successful cases versus failed cases for the source-sink model whereas the distributions obtained using HFO rate overlap and consequently the predictive power of HFO rates is lower. B. Distributions of p_s stratified by Engel Class (Engel I = successful outcome, Engel 2-4 = failed outcome). For the source-sink metrics, there is a general trend of decreasing $p_s$values as the Engel class (and thus also severity of surgical outcome) increases. In contrast, this does not hold for the HFO rate. C. Distributions of p_s stratified by ILAE scores (ILAE 1-2 = successful outcome, ILAE3-5 = failed outcome) follow a similar trend to those observed for the Engel class in B. S = successful surgical outcome, F = failed surgical outcome.

bioRxiv preprint doi: https://doi.org/10.1101/2021.10.15.464594; this version posted October 18, 2021. The copyright holder for this preprint (which was not certified by peer review) is the author/funder. All rights reserved. No reuse allowed without permission.

Top SSI regions have high correspondence to CA-EZ in success patients but lower in failed patients

The treating neurologist at each center was given the SS-maps for each patient from the corresponding center and asked to rate the clinical correspondence between the CA-EZ and regions with top SSIs. Fig. 7 shows the clinical correspondence scores between the two sets of EZ regions for success versus failure patients across all centers. Correspondence scores of "some" or "strong" agreement were lumped into "agreement" for visualization purposes. In general, there was more agreement between the CA-EZ and regions with high SSIs in patients with successful outcomes compared to patients with failed surgical outcomes, which means that the source-sink analysis often highlighted other, non-treated potential onset regions, in failure patients. In fact, clinicians agreed with the algorithm in 26 out of 28 (93%) patients, whereas only 54% of patients with failed outcomes were considered in agreement. When categorized by Engel scores, the rate of agreement decreased as the Engel class increased, which likely also reflects the increased difficulty of treatment in these patients. A similar trend was observed for the ILAE scores, with a higher rate of disagreement corresponding to a higher ILAE score.

bioRxiv preprint doi: https://doi.org/10.1101/2021.10.15.464594; this version posted October 18, 2021. The copyright holder for this preprint (which was not certified by peer review) is the author/funder. All rights reserved. No reuse allowed without permission.

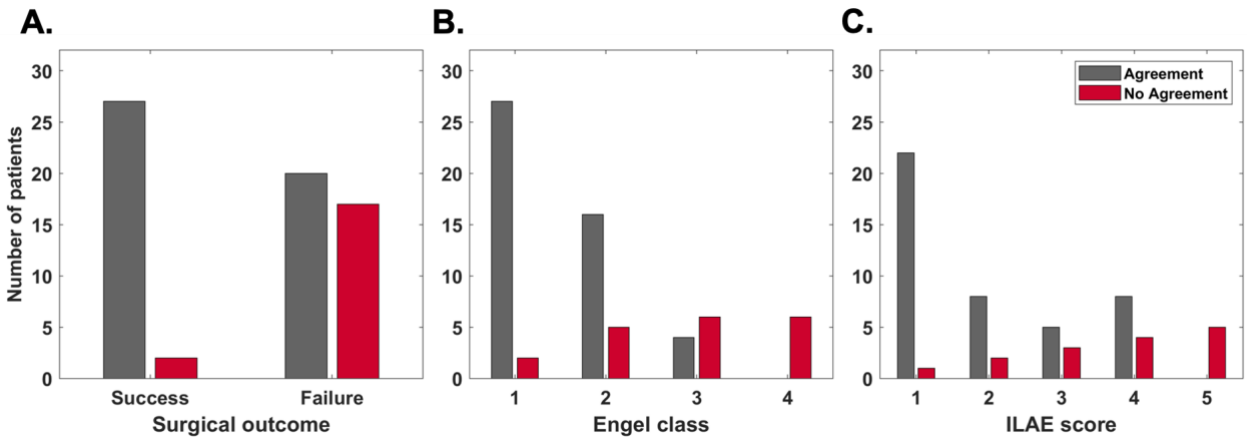

Figure 7. Clinical correspondence between CA-EZ and top SSI regions. A. Clinical correspondence stratified by surgical outcome. For almost all success patients, clinicians agree with the channels with highest SSI scores. The agreement is much lower in failure patients. Note that in some failure patients, clinicians may not be able to treat all or a proportion the CA-EZ (e.g., if it is located in eloquent cortex). In those cases, the source-sink algorithm may agree with clinicians even though the patient had a failed surgical outcome. B. Clinical correspondence stratified by Engel class. The rate of agreement is highest for Engel 1 (complete seizure-freedom) but decreases as the Engel class increases. No agreement scores follow the opposite trend. C. Clinical correspondence stratified by ILAE scores follow an overall similar trend with decreasing agreement (and increasing disagreement) as ILAE score increases.

CA-EZ regions are sinks at rest but become sources during seizures in success patients

In addition to computing the source-sink metrics across interictal recordings, we also investigated source-sink properties of the iEEG network during ictal periods. We did not receive ictal snapshots from all centers, so only a subset of the patient population ($n = 29$) was included in this part of the analysis. Fig. 8 demonstrates the source-sink characteristics of the iEEG network as the brain moves from resting state (interictal) towards a seizure in one success (A) and one failure (B) patient. For each patient, we computed each iEEG channel's SSI in 500-msec windows of one interictal and one ictal recording. Note that the two snapshots are not consecutive in time as the interictal snapshot is typically recorded hours before the seizure event. As Fig. 8A shows, the CA-EZ channels have a high SSI in the success patient during rest, suggesting they are top sinks strongly influenced by top sources. However, during

bioRxiv preprint doi: https://doi.org/10.1101/2021.10.15.464594; this version posted October 18, 2021. The copyright holder for this preprint (which was not certified by peer review) is the author/funder. All rights reserved. No reuse allowed without permission.

and right after seizure, the same channels have a low SSI, that is, they are exhibiting a strong source-like behavior, which further supports the source-sink hypothesis. In contrast, only a small subset of CA-EZ channels (2 out of 13) are amongst the top sinks in the patient with a failed surgical outcome (Fig. 8B) and there is little modulation of the SSI of these channels.

The temporal SSI modulation is summarized in Fig. 8C and D. We computed the average source-sink index for two groups of interest: i) CA-EZ channels, and ii) all other channels not labeled as CA-EZ (CA-NEZ). Each curve was obtained by computing the average source-sink index of each channel group, in each window. The curves were smoothed by computing the index across 10-second windows instead of 500 msec. As Fig. 8C shows, the CA-EZ channels have a much higher SSI compared to the rest of the network during the interictal period. However, this does not hold true for the failure patient (Fig. 8D), where the mean index of the CA-EZ is not separable, or even slightly lower than the mean index of the CA-NEZ channels.

bioRxiv preprint doi: https://doi.org/10.1101/2021.10.15.464594; this version posted October 18, 2021. The copyright holder for this preprint (which was not certified by peer review) is the author/funder. All rights reserved. No reuse allowed without permission.

Fig. 8E and F show an example of the 2D source-sink space for the success and failure patients, respectively, computed in 10-second windows at different points in time relative to seizure onset. Despite the temporal stability of the source-sink metrics across interictal recordings, the source-sink properties of the iEEG network modulate around seizure events. In success patients (Fig. 8E) we frequently observed a movement of CA-EZ towards top sources as the brain

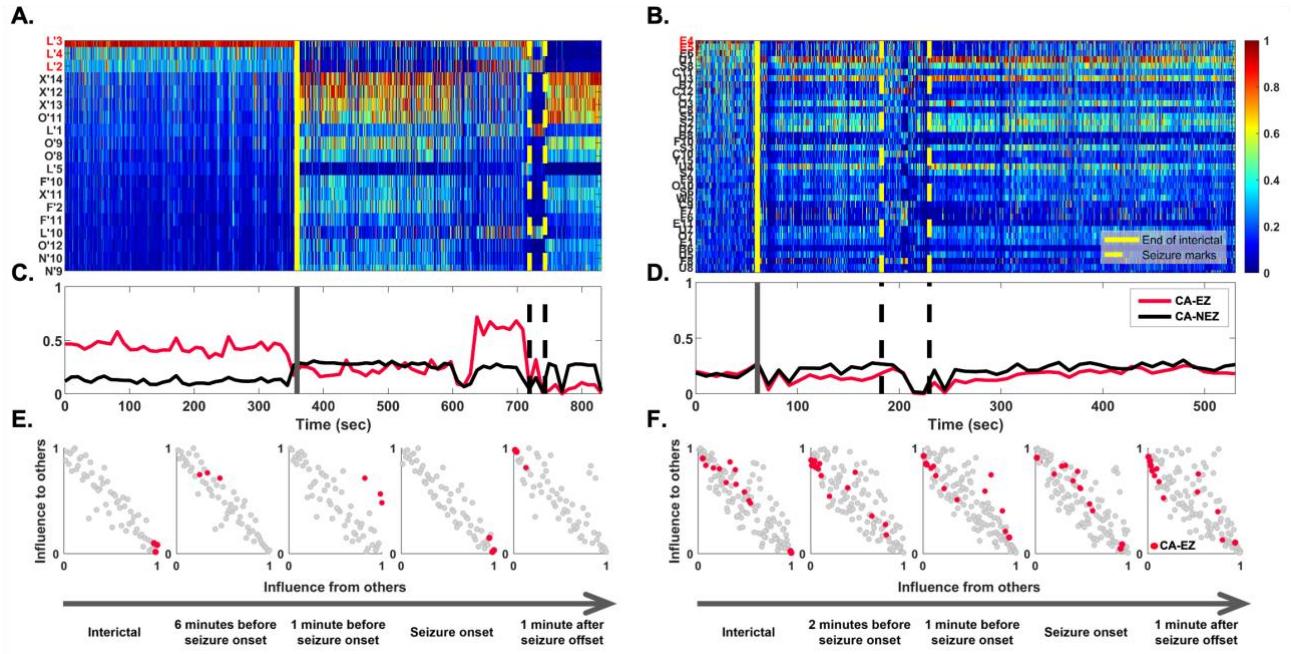

Figure 8. Source-sink characteristics as the brain moves from resting state towards a seizure. Two patient examples. A. Source-sink index of every channel during interictal (left) and ictal (right) periods, separated by the solid yellow line. Channels are arranged from highest to lowest average interictal SSI. CA-EZ channels are colored red. Only the top 30% of channels are shown for better visualization purposes, and all channels not shown have low SSI values. B. Average source-sink index of four CA-EZ versus CA-NEZ channels. In this success patient the CA-EZ channels have a much higher SSI compared to CA-NEZ channels during the interictal period. The SSI of CA-EZ channels drops significantly during seizure, as these channels become sources to initiate and spread seizure activity. D. Source-sink index of every channel over time. Only 2 out of 13 CA-EZ channels have a high source-sink index in this failure patient. E. Average source-sink index of the two groups. In this failure patient CA-EZ cannot be distinguished from CA-NEZ. E. Movement of CA-EZ channels in the 2D source-sink space over time. CA-EZ channels are top sinks during the interictal period (left), but move towards sources as the brain progresses towards a seizure. F. In this failure patient, there is little movement of CA-EZ channels as the brain moves from interictal to ictal state.

progresses towards a seizure. Right before and at the onset of seizure however, the CA-EZ channels become sinks for a short period, perhaps as the rest of the network makes one last attempt to prevent the seizure from starting. During and right after seizure, the CA-EZ channels

bioRxiv preprint doi: https://doi.org/10.1101/2021.10.15.464594; this version posted October 18, 2021. The copyright holder for this preprint (which was not certified by peer review) is the author/funder. All rights reserved. No reuse allowed without permission.

are again exhibiting a strong source-like behavior. The same cannot be said about the CA-EZ channels in failure patients (Fig. 8F), where there was little movement of these channels in the SS-map over time.

Finally, Fig. 9 compares the temporal SSI modulation in success versus failure patients. For each patient, SSI was computed in four predefined windows: a) a 30 second window of the interictal recording, b) 60-30 seconds before the seizure event, c) during the seizure event, and d) 60-90 seconds after the end of seizure. For each set of channels, indices were normalized to the average SSI of the entire network at rest (window a). At each time point, we then computed the mean ± standard error of SSI across all success patients ($n = 14$) and all failure patients ($n = 15$). In the success patients, (Fig. 9, top) the CA-EZ have a significantly higher SSI compared to the rest of the channels in the network in all windows except after the end of seizure ($p_a = 0.0132, p_b = 0.0029, p_c = 0.0015, p_d = 0.4240$). In contrast, the CA-EZ channels are not separable from the CA-NEZ channels at any time point ($p_{a,b,c,d} \gg 0.05$) in failure patients.

bioRxiv preprint doi: https://doi.org/10.1101/2021.10.15.464594; this version posted October 18, 2021. The copyright holder for this preprint (which was not certified by peer review) is the author/funder. All rights reserved. No reuse allowed without permission.

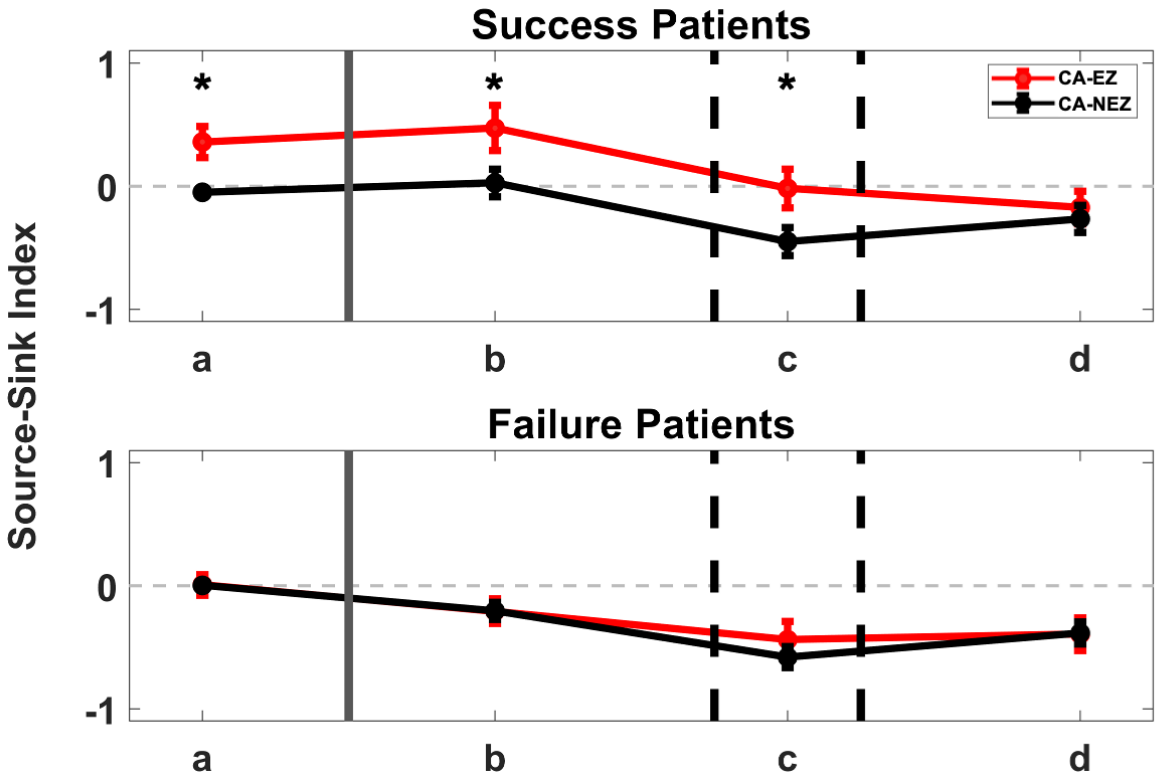

Figure 9. Temporal SSI modulation in CA-EZ versus CA-NEZ channels. Indices were averaged over all CA-EZ and all CA-NEZ for each patient. Each curve shows the mean ± s.d. across 14 success patients (top) and 15 failure patients (bottom). CA-EZ channels have a higher SSI compared to CA-NEZ channels in success patients, but not in failure patients. The asterisks indicate a statistically significant difference between CA-EZ and CA-NEZ channels. a = 30 second window of the interictal recording, b = 60-30 seconds before the seizure event, c = during the seizure event, and d = 60-90 seconds after the end of seizure.

Discussion

We proposed a novel source-sink index as a dynamical-network-based interictal iEEG marker to assist in the localization of the EZ. The index was developed based on the hypothesis that seizures are suppressed when the epileptogenic regions are effectively being inhibited by neighboring regions. The source-sink hypothesis is supported by clinical evidence based on the levels of glutamate and glutamate receptors in the brain[55–58] and iEEG studies that have demonstrated strong inward (inhibitory) connectivity to the EZ regions during rest.[59,60,63,64] We evaluated the predictive value of the SSI by a) rating the correspondence between the

bioRxiv preprint doi: https://doi.org/10.1101/2021.10.15.464594; this version posted October 18, 2021. The copyright holder for this preprint (which was not certified by peer review) is the author/funder. All rights reserved. No reuse allowed without permission.

hypothesized CA-EZ and regions with high SSIs and b) building a random forest to model the probability of a successful surgery as a function of the source-sink metrics, and compared the performance to that of HFOs, a commonly used interictal iEEG feature. The analysis was performed on data from 65 patients treated across 6 clinical centers. Out of 28 success patients in our dataset, the source-sink algorithm agreed (rated as "*strong"* or *"some"* agreement) with clinicians in 26 (93%) of patients. In contrast, only 54% of patients with failed outcomes were considered in agreement with clinicians, suggesting that in failure patients, the source-sink algorithm highlighted other areas than the ones identified and treated as potentially epileptogenic. Further, in terms of predicting surgical outcomes, the source-sink metrics outperformed HFO rate, with higher AUC, accuracy, precision, sensitivity and specificity, predicting 79% outcomes correctly compared to a 65% accuracy of the HFO model.

Challenges

Validating iEEG markers of the EZ

At present, identification of the EZ is a complicated and subjective process that is often unsuccessful, thus resulting in post-treatment recurrence of seizure activity in a large proportion of patients. In order to increase the likelihood of a successful treatment outcome, there is a great need to identify and validate reliable biomarkers that can determine the extent and location of the EZ with high precision and accuracy. However, validation of such markers remains challenging because the EZ is a theoretical concept that cannot be directly measured[15] and thus no ground truth of its exact location exists. Instead, the best estimate one can obtain is retrospectively, by assuming the EZ was included in the resected cortex if surgical treatment renders the patient seizure free. To complicate matters even further, a complete removal of the EZ is not the only basis of a successful surgery and although removing the EZ is typically

bioRxiv preprint doi: https://doi.org/10.1101/2021.10.15.464594; this version posted October 18, 2021. The copyright holder for this preprint (which was not certified by peer review) is the author/funder. All rights reserved. No reuse allowed without permission.

necessary to achieve lasting seizure freedom, it may not always be sufficient (e.g., a disconnection of the EZ from the early spread regions may also produce good outcomes). Post-operative outcome measures (e.g., Engel scores) are also based on subjective judgement and may be interpreted differently from center to center. Consequently, results from different centers cannot be compared easily.[48] Further, insufficient sampling of electrodes may also lead to inaccurate results as there is no way for the iEEG marker to capture the EZ if it is not covered, but this is a limitation of all computational approaches. In the case of the source-sink algorithm, the results may also be less accurate if the sources, i.e., the regions inhibiting the EZ, are not covered.

Why the source-sink algorithm may disagree with clinicians in success patients

For a majority of success patients, the source-sink algorithm was in agreement with the clinicians regarding the location of the EZ (Fig. 7), and only 2 out of 28 success patients were deemed in disagreement. In addition to completely removing the EZ, a disconnection of the EZ from the rest of the epileptogenic network or removal of the regions responsible for early spread of the seizure activity may also lead to a successful surgical outcome. Thus, it is possible that in those patients, the treated areas may have included the early spread regions instead of the onset zone and therefore are not overlapping with the areas highlighted by the source-sink algorithm.

Why the source-sink algorithm may agree with clinicians in failure patients

With that said, surgical treatment may also fail for various reasons and in more complex cases, removing the EZ may not be sufficient to achieve seizure freedom. Further, in some patients, new regions may become epileptogenic post-surgery. Consequently, the source-sink algorithm

bioRxiv preprint doi: https://doi.org/10.1101/2021.10.15.464594; this version posted October 18, 2021. The copyright holder for this preprint (which was not certified by peer review) is the author/funder. All rights reserved. No reuse allowed without permission.

may be in full or some agreement with the treated areas, even in patients with failed outcomes. Additionally, incorrect or inaccurate localization of the EZ and incomplete treatment of these regions most likely leads to seizure recurrence after surgery. This can occur in cases where the implanted electrodes are not covering the true EZ, in which case it is impossible (for clinicians and algorithms) to detect the true EZ, or if the EZ is widely spread. Finally, in some patients, a complete resection of the EZ cannot be performed without causing a new, unacceptable deficit to the patient (e.g., if the EZ is located in eloquent cortex). Instead, palliative treatments, including RNS or deep brain stimulation, have been increasingly used in patients who are not candidates for resective surgery. These treatments can be effective in reducing seizure frequency, but only a minority of patients experience complete seizure control.[73–75]

Other interictal iEEG markers of the EZ

The current gold standard visual analysis of hundreds of iEEG recordings to localize the EZ is time consuming and subject to individual expert biases. Although many interictal iEEG markers of the EZ have been proposed, no computational tools are used in the clinical workflow today to specifically assist in localizing the EZ. With epilepsy increasingly understood as a network disorder,[19–22] a profound knowledge of the underlying network dynamics and interactions between brain regions is essential to understand how the internal properties of the brain network can generate or prevent seizures. An important limitation of the majority of proposed algorithms lies in the fact that they fail to capture these internal properties of the iEEG network. Instead, most existing methods either compute single-channel-based iEEG features such as spectral power in frequency bands, spike counts or HFO rates (e.g., [34,38,40,41,43–45,76–78]), thus not capturing dependencies between channels, or they apply network-based measures ([20,21,32–37,79–81] to name a few) to capture pairwise dependencies (correlation or coherence) between the iEEG channels, but fail to characterize the underlying dynamics of the

bioRxiv preprint doi: https://doi.org/10.1101/2021.10.15.464594; this version posted October 18, 2021. The copyright holder for this preprint (which was not certified by peer review) is the author/funder. All rights reserved. No reuse allowed without permission.

network. Network-based measures (e.g., node centrality, degree distributions or distance measures) are summary statistics computed from an adjacency matrix that is used to represent the pairwise dependencies between any two iEEG channels. The main downside of these however, is that each network can be mapped to multiple adjacency matrices (because connectivity between two nodes can be defined in numerous ways), and many different adjacency matrices can have identical summary statistics. Thus, such metrics are not based on well formulated hypotheses of the role of the EZ in the network and are not easily interpretable either.

HFOs are some of the most studied iEEG features as a potential interictal marker of the EZ (e.g. [38,41,42,45,67,82–96]). In the context of epilepsy, there is evidence that regions that belong to the EZ have higher HFO rates compared to non-epileptogenic regions[82] and studies have suggested that removal of regions that generate high rates of HFOs correlates with good post-surgical outcome.[42,83,84,86–88,95,96] However, there still remains considerable controversy surrounding HFOs as a valid marker of the EZ. Other studies have not found a predictive value in the removal of these regions[84,88] and two meta-analyses of existing studies concluded that the evidence of HFOs as a predictor of surgical outcome is weak.[85,97]

Furthermore, several studies have also questioned the reproducibility and reliability of HFOs as a marker.[46,87,88,98,99] First, no consensus has been reached on the exact features used to describe HFOs, because the exact underlying cellular mechanism by which they are generated remains unknown,[87] which gives rise to variability in the features chosen to define HFOs among current studies.[100] Second, HFOs can also occur in non-epileptogenic regions and even in patients without epilepsy.[46] These physiologic, non-epileptic HFOs have features that overlap with those of pathological HFOs[101–103] and differentiation between the two types remains an unresolved issue in iEEG studies.[104–107]

bioRxiv preprint doi: https://doi.org/10.1101/2021.10.15.464594; this version posted October 18, 2021. The copyright holder for this preprint (which was not certified by peer review) is the author/funder. All rights reserved. No reuse allowed without permission.

Finally, HFO rates are not stable over time. Gliske et al. tested the consistency of channels exhibiting the highest number of HFOs across different 10-minute segments of data.[46] They showed that the location of the highest HFO-rate channels varied greatly when different segments were used, thus questioning the reliability of such marker. In contrast, we showed above that the source-sink analysis returns consistent results independent of recording length and is in fact, robust to any random selection of interictal activity (Fig.4). Further, we repeated the analysis with and without the removal of large artifacts from the SEEG snapshots and found that the results held regardless.

Translating an iEEG marker into the clinical workflow

In order to translate an iEEG marker of the EZ into clinical workflow, it is critical to perform rigorous testing and validation to ensure the marker meets the stringent criteria needed for it to serve as a reliable source of information for clinical decision making. We sought to evaluate the performance of the SSI on a diverse group of patients, reflecting different epilepsy etiologies, treatment methods and post-treatment outcomes. We collected our iEEG data from six different clinical centers. As such, our dataset is comprised of a heterogeneous patient population, spanning varying case complexities (such as lesional or non-lesional, and temporal or extra-temporal epilepsy), epilepsy types (focal and multi-focal) and clinical practices, while at the same time reflecting the standard of care success rates of approximately 50% on average.

Generalizability of the SSI

In order to properly validate any biomarker, it is important to determine the range of conditions under which it will give reproducible and accurate results. Similarly, a profound understanding of when the tool performs well and when and why it fails is critical. For example, some patients present with a lower clinical case complexity (such as a visible lesion on MRI or some types

bioRxiv preprint doi: https://doi.org/10.1101/2021.10.15.464594; this version posted October 18, 2021. The copyright holder for this preprint (which was not certified by peer review) is the author/funder. All rights reserved. No reuse allowed without permission.

of temporal epilepsy) and have as such higher chances of good surgical outcomes. A tool that performs well on these patients is not guaranteed to translate well to more complex cases. Importantly, although not shown here, we show in Appendix 2.3 (Supplementary Figs. 3-6) that the SSI is agnostic to the clinical complexity of each patient (as defined by our clinical team) as well as treatment methods, suggesting that the tool is highly generalizable. Further, the performance was very similar across all centers (Supplementary Figs. 4 and 5), indicating that the tool generalized well across different datasets and the overall probabilities and scores were not biased by any particular center.

Conclusions and future work

Due to the spatial resolution of the iEEG contacts, the DNMs cannot distinguish between excitatory and inhibitory connections and thus the only information we can glean from the models is the amount of influence between any two nodes in the network. The high predictive performance of the SSI does however suggest that the sources are likely dominated by inhibitory influence, consistent with the source-sink hypothesis. To better understand the excitatory or inhibitory nature of the connections, future work may entail complementing the iEEG data with resting-state fMRI (rs-fMRI), which has a poorer temporal resolution, but generally a higher spatial resolution compared to iEEG.[108] Thus combining iEEG and rs-fMRI could provide a better understanding of the directionality of the network connections.[109]

In patients with electrodes targeting the hippocampal region, the hippocampal contacts were frequently identified as top sinks in the iEEG network. The hippocampus is a highly connected structure, with many bidirectional connections within and to surrounding regions[110] both intra- and inter-hemispherically.[111] Further, studies of mesial temporal lobe epilepsy (MTLE) have demonstrated the existence of strong connections within the hippocampal network bilaterally in both epileptogenic as well as non-epileptogenic hippocampi.[110,112,113] As such, the

bioRxiv preprint doi: https://doi.org/10.1101/2021.10.15.464594; this version posted October 18, 2021. The copyright holder for this preprint (which was not certified by peer review) is the author/funder. All rights reserved. No reuse allowed without permission.

hippocampus is a structure that is highly influenced by other regions and by its nature acts as a sink in the brain network regardless of its epileptogenicity. Moreover, we found that in MTLE patients, contacts recording from the contralateral hippocampus commonly exhibited a stronger sink-like behavior than the epileptogenic hippocampus. This connectivity asymmetry across hemispheres is in line with findings of other studies, which have demonstrated a decreased functional connectivity within the epileptogenic hippocampal networks with a concurrent increased connectivity in contralateral hippocampal pathways, possibly reflecting compensatory mechanisms with strengthening of alternative pathways in these patients.[110,114–116] To that end, the connectivity patterns and natural sink-like behavior of the hippocampus need to be taken into consideration as results of the source-sink analysis are reviewed and interpreted. Although the tool performs well with the hippocampal electrodes included in the datasets, as reflected by our results, there might be cases where these electrodes could simply be removed (e.g., clinical experts are certain that the hippocampus is not involved in seizure onset – and hippocampus was only targeted to rule out temporal epilepsy or determine spread – and thus would ignore these electrodes in their standard of care analyses). Our preliminary testing has showed that inclusion or removal of hippocampal electrodes does not alter the source-sink behavior of other contacts in the iEEG network and thus, a future augmentation of the tool could include an option to remove the hippocampal electrodes before the visual interpretation of the source-sink results is performed by clinicians.

Finally, the algorithm was developed and validated on adult patients only. Although we expect the results to hold in the pediatric population, an important next step would be a robust evaluation of the SSI on interictal iEEG data from a large population of children with MRE.

In conclusion, our results suggest that the SSI, a metric entirely based on the properties of the iEEG network at rest, captures the characteristics of the regions responsible for seizure initiation. SSI is a promising marker of the EZ and could significantly improve surgical

bioRxiv preprint doi: https://doi.org/10.1101/2021.10.15.464594; this version posted October 18, 2021. The copyright holder for this preprint (which was not certified by peer review) is the author/funder. All rights reserved. No reuse allowed without permission.

outcomes by increasing the precision of EZ localization. Furthermore, by removing the need to capture seizures, the tool has the potential to substantially reduce invasive monitoring times, avoiding further risks to patients and reducing costs to hospitals.

Funding

KMG was supported by a grant from the American Epilepsy Society. SVS is supported by ….. Ask Stephanie to mention my R21 with Daniel. Ask co-authors for theirs.

Competing interests

This section is mandatory. If there are no competing interests, the following declaration should be added: 'The authors report no competing interests.'

Supplementary material

Supplementary material is available at *Brain* online.

References

1. Fiest KM, Sauro KM, Wiebe S, et al. Prevalence and incidence of epilepsy. *Neurology*. 2017;88(3):296. doi:10.1212/WNL.0000000000003509

2. Kwan P, Brodie MJ. Definition of refractory epilepsy: defining the indefinable? *Lancet Neurol*. 2010;9(1):27-29. doi:10.1016/S1474-4422(09)70304-7

3. Berg AT, Kelly MM. Defining intractability: comparisons among published definitions. *Epilepsia*. 2006;47(2):431-436. doi:10.1111/j.1528-1167.2006.00440.x

4. Kwan P, Sander JW. The natural history of epilepsy: an epidemiological view. *J Neurol Neurosurg Psychiatry*. 2004;75(10):1376-1381. doi:10.1136/jnnp.2004.045690

5. Laxer KD, Trinka E, Hirsch LJ, et al. The consequences of refractory epilepsy and its treatment. *Epilepsy Behav*. 2014;37:59-70. doi:10.1016/j.yebeh.2014.05.031

6. Murray MI, Halpern MT, Leppik IE. Cost of refractory epilepsy in adults in the USA. *Epilepsy Res*. 1996;23(2):139-148. doi:10.1016/0920-1211(95)00090-9

7. Begley CE, Famulari M, Annegers JF, et al. The cost of epilepsy in the United States: an estimate from population-based clinical and survey data. *Epilepsia*. 2000;41(3):342-351.

bioRxiv preprint doi: https://doi.org/10.1101/2021.10.15.464594; this version posted October 18, 2021. The copyright holder for this preprint (which was not certified by peer review) is the author/funder. All rights reserved. No reuse allowed without permission.

8. Begley CE, Durgin TL. The direct cost of epilepsy in the United States: A systematic review of estimates. *Epilepsia*. 2015;56(9):1376-1387. doi:10.1111/epi.13084

9. Ferro MA, Speechley KN. Stability of latent classes in group-based trajectory modeling of depressive symptoms in mothers of children with epilepsy: An internal validation study using a bootstrapping procedure. *Soc Psychiatry Psychiatr Epidemiol*. 2013;48(7):1077-1086. doi:10.1007/s00127-012-0622-6

10. Strzelczyk A, Griebel C, Lux W, Rosenow F, Reese J-P. The Burden of Severely Drug-Refractory Epilepsy: A Comparative Longitudinal Evaluation of Mortality, Morbidity, Resource Use, and Cost Using German Health Insurance Data. *Front Neurol*. 2017;8. doi:10.3389/fneur.2017.00712

11. Beghi E. Addressing the burden of epilepsy: Many unmet needs. *Pharmacol Res*. 2016;107:79-84. doi:10.1016/j.phrs.2016.03.003

12. Lüders HO, Najm I, Nair D, Widdess-Walsh P, Bingman W. The epileptogenic zone: general principles. *Epileptic Disord*. 2006;8(2):1-9.

13. Jeha LE, Najm I, Bingaman W, Dinner D, Widdess-Walsh P, Lüders H. Surgical outcome and prognostic factors of frontal lobe epilepsy surgery. *Brain*. 2007;130(2):574-584. doi:10.1093/brain/awl364

14. Ramey WL, Martirosyan NL, Lieu CM, Hasham HA, Lemole GM, Weinand ME. Current management and surgical outcomes of medically intractable epilepsy. *Clin Neurol Neurosurg*. 2013;115(12):2411-2418. doi:10.1016/j.clineuro.2013.09.035

15. Rosenow F, Lüders H. Presurgical evaluation of epilepsy. *Brain*. 2001;124(9):1683-1700. doi:10.1093/brain/124.9.1683

16. Dubeau F, McLachlan RS. Invasive Electrographic Recording Techniques in Temporal Lobe Epilepsy. *Can J Neurol Sci*. 2000;27(S1):S29-S34. doi:10.1017/S0317167100000615

17. Jung WY, Pacia SV, Devinsky O. Neocortical temporal lobe epilepsy: intracranial EEG features and surgical outcome. *J Clin Neurophysiol Off Publ Am Electroencephalogr Soc*. 1999;16(5):419-425. doi:10.1097/00004691-199909000-00003

18. Bulacio JC, Chauvel P, McGonigal A. Stereoelectroencephalography: Interpretation. *J Clin Neurophysiol*. 2016;33(6):503-510. doi:10.1097/WNP.0000000000000305

19. Bernhardt BC, Bonilha L, Gross DW. Network analysis for a network disorder: The emerging role of graph theory in the study of epilepsy. *Epilepsy Behav*. 2015;50:162-170. doi:10.1016/j.yebeh.2015.06.005

20. Li A, Chennuri B, Subramanian S, et al. Using network analysis to localize the epileptogenic zone from invasive EEG recordings in intractable focal epilepsy. *Netw Neurosci*. 2018;2(2):218-240. doi:10.1162/netn_a_00043

21. Bassett DS, Sporns O. Network neuroscience. *Nat Neurosci*. 2017;20(3):353-364. doi:10.1038/nn.4502

bioRxiv preprint doi: https://doi.org/10.1101/2021.10.15.464594; this version posted October 18, 2021. The copyright holder for this preprint (which was not certified by peer review) is the author/funder. All rights reserved. No reuse allowed without permission.

22. Stacey W, Kramer M, Gunnarsdottir K, et al. Emerging roles of network analysis for epilepsy. *Epilepsy Res*. 2020;159:106255. doi:10.1016/j.eplepsyres.2019.106255

23. Nair DR, Burgess R, McIntyre CC, Lüders H. Chronic subdural electrodes in the management of epilepsy. *Clin Neurophysiol*. 2008;119(1):11-28. doi:10.1016/j.clinph.2007.09.117

24. Li A, Huynh C, Fitzgerald Z, et al. Neural fragility as an EEG marker of the seizure onset zone. *Nat Neurosci*. Published online August 5, 2021:1-10. doi:10.1038/s41593-021-00901-w

25. Bartolomei F, Chauvel P, Wendling F. Epileptogenicity of brain structures in human temporal lobe epilepsy: a quantified study from intracerebral EEG. *Brain J Neurol*. 2008;131(Pt 7):1818-1830. doi:10.1093/brain/awn111

26. Gnatkovsky V, Francione S, Cardinale F, et al. Identification of reproducible ictal patterns based on quantified frequency analysis of intracranial EEG signals. *Epilepsia*. 2011;52(3):477-488. doi:10.1111/j.1528-1167.2010.02931.x

27. Mierlo P van, Carrette E, Hallez H, et al. Ictal-onset localization through connectivity analysis of intracranial EEG signals in patients with refractory epilepsy. *Epilepsia*. 2013;54(8):1409-1418. doi:10.1111/epi.12206

28. David O, Blauwblomme T, Job A-S, et al. Imaging the seizure onset zone with stereo-electroencephalography. *Brain*. 2011;134(10):2898-2911. doi:10.1093/brain/awr238

29. Schindler K, Rummel C, Andrzejak RG, et al. Ictal time-irreversible intracranial EEG signals as markers of the epileptogenic zone. *Clin Neurophysiol*. 2016;127(9):3051-3058. doi:10.1016/j.clinph.2016.07.001

30. Bou Assi E, Rihana S, Nguyen DK, Sawan M. Effective connectivity analysis of iEEG and accurate localization of the epileptogenic focus at the onset of operculo-insular seizures. *Epilepsy Res*. 2019;152:42-51. doi:10.1016/j.eplepsyres.2019.02.006

31. Quitadamo LR, Foley E, Mai R, de Palma L, Specchio N, Seri S. EPINETLAB: A Software for Seizure-Onset Zone Identification From Intracranial EEG Signal in Epilepsy. *Front Neuroinformatics*. 2018;12. doi:10.3389/fninf.2018.00045

32. Shah P, Ashourvan A, Mikhail F, et al. Local structural connectivity directs seizure spread in focal epilepsy. *bioRxiv*. Published online September 4, 2018:406793. doi:10.1101/406793

33. Li Y-H, Ye X-L, Liu Q-Q, et al. Localization of epileptogenic zone based on graph analysis of stereo-EEG. *Epilepsy Res*. 2016;128:149-157. doi:10.1016/j.eplepsyres.2016.10.021

34. Cimbalnik J, Klimes P, Sladky V, et al. Multi-feature localization of epileptic foci from interictal, intracranial EEG. *Clin Neurophysiol*. 2019;130(10):1945-1953. doi:10.1016/j.clinph.2019.07.024

35. Dauwels J, Eskandar E, Cash S. Localization of seizure onset area from intracranial non-seizure EEG by exploiting locally enhanced synchrony. In: *2009 Annual International*

bioRxiv preprint doi: https://doi.org/10.1101/2021.10.15.464594; this version posted October 18, 2021. The copyright holder for this preprint (which was not certified by peer review) is the author/funder. All rights reserved. No reuse allowed without permission.

Conference of the IEEE Engineering in Medicine and Biology Society. ; 2009:2180-2183. doi:10.1109/IEMBS.2009.5332447

36. Ortega GJ, Menendez de la Prida L, Sola RG, Pastor J. Synchronization clusters of interictal activity in the lateral temporal cortex of epileptic patients: intraoperative electrocorticographic analysis. *Epilepsia*. 2008;49(2):269-280. doi:10.1111/j.1528-1167.2007.01266.x

37. Monto S, Vanhatalo S, Holmes MD, Palva JM. Epileptogenic Neocortical Networks Are Revealed by Abnormal Temporal Dynamics in Seizure-Free Subdural EEG. *Cereb Cortex*. 2007;17(6):1386-1393. doi:10.1093/cercor/bhl049

38. Gliske SV, Irwin ZT, Davis KA, Sahaya K, Chestek C, Stacey WC. Universal automated high frequency oscillation detector for real-time, long term EEG. *Clin Neurophysiol*. 2016;127(2):1057-1066. doi:10.1016/j.clinph.2015.07.016

39. Nariai H, Hussain SA, Bernardo D, et al. Prospective observational study: Fast ripple localization delineates the epileptogenic zone. *Clin Neurophysiol*. 2019;130(11):2144-2152. doi:10.1016/j.clinph.2019.08.026

40. Varatharajah Y, Berry B, Cimbalnik J, et al. Integrating artificial intelligence with real-time intracranial EEG monitoring to automate interictal identification of seizure onset zones in focal epilepsy. *J Neural Eng*. 2018;15(4):046035. doi:10.1088/1741-2552/aac960

41. Murphy PM, von Paternos AJ, Santaniello S. A novel HFO-based method for unsupervised localization of the seizure onset zone in drug-resistant epilepsy. In: *2017 39th Annual International Conference of the IEEE Engineering in Medicine and Biology Society (EMBC)*. ; 2017:1054-1057. doi:10.1109/EMBC.2017.8037008

42. Akiyama T, McCoy B, Go CY, et al. Focal resection of fast ripples on extraoperative intracranial EEG improves seizure outcome in pediatric epilepsy. *Epilepsia*. 2011;52(10):1802-1811. doi:10.1111/j.1528-1167.2011.03199.x

43. Conrad EC, Tomlinson SB, Wong JN, et al. Spatial distribution of interictal spikes fluctuates over time and localizes seizure onset. *Brain*. 2020;143(2):554-569. doi:10.1093/brain/awz386

44. Gaspard N, Alkawadri R, Farooque P, Goncharova II, Zaveri HP. Automatic detection of prominent interictal spikes in intracranial EEG: Validation of an algorithm and relationsip to the seizure onset zone. *Clin Neurophysiol*. 2014;125(6):1095-1103. doi:10.1016/j.clinph.2013.10.021

45. Wang S, Wang IZ, Bulacio JC, et al. Ripple classification helps to localize the seizure-onset zone in neocortical epilepsy. *Epilepsia*. 2013;54(2):370-376. doi:10.1111/j.1528-1167.2012.03721.x

46. Gliske SV, Irwin ZT, Chestek C, et al. Variability in the location of high frequency oscillations during prolonged intracranial EEG recordings. *Nat Commun*. 2018;9(1):2155. doi:10.1038/s41467-018-04549-2

bioRxiv preprint doi: https://doi.org/10.1101/2021.10.15.464594; this version posted October 18, 2021. The copyright holder for this preprint (which was not certified by peer review) is the author/funder. All rights reserved. No reuse allowed without permission.

47. J Engel Jr., PC Van Ness, TB Rasmussen, LM Ojemann. Outcome with respect to epileptic seizures. In: J Engel Jr., ed. *Surgical Treatment of the Epilepsies*. Raven Press; 1993:609-621.

48. Wieser H, Blume W, Fish D, et al. ILAE Commission Report: Proposal for a New Classification of Outcome with Respect to Epileptic Seizures Following Epilepsy Surgery. *Epilepsia*. 2001;42(2):282-286.

49. Li LM, Cendes F, Andermann F, et al. Surgical outcome in patients with epilepsy and dual pathology. *Brain*. 1999;122(5):799-805. doi:10.1093/brain/122.5.799

50. Sheikh S, Thompson N, Bingaman W, Gonzalez-Martinez J, Najm I, Jehi L. (Re)Defining success in epilepsy surgery: The importance of relative seizure reduction in patient-reported quality of life. *Epilepsia*. 2019;60(10):2078-2085. doi:10.1111/epi.16327

51. Immonen A, Jutila L, Muraja-Murro A, et al. Long-term epilepsy surgery outcomes in patients with MRI-negative temporal lobe epilepsy. *Epilepsia*. 2010;51(11):2260-2269. doi:10.1111/j.1528-1167.2010.02720.x

52. Elsharkawy AE, Behne F, Oppel F, et al. Long-term outcome of extratemporal epilepsy surgery among 154 adult patients. *J Neurosurg*. 2008;108(4):676-686. doi:10.3171/JNS/2008/108/4/0676

53. Zhukov L, Weinstein D. Independent Component Analysis for EEG Source Localization in Realistic Head Models. *IEEE Eng Med Biol Mag Q Mag Eng Med Biol Soc*. 2000;19:87-96. doi:10.1109/51.844386

54. Zhou Y, Danbolt N. Glutamate as a neurotransmitter in the healthy brain. *J Neural Transm*. 2014;121(8):799-817. doi:10.1007/s00702-014-1180-8

55. Greenamyre JT. The role of glutamate in neurotransmission and in neurologic disease. *Arch Neurol*. 1986;43(10):1058-1063. doi:10.1001/archneur.1986.00520100062016

56. Zhang WQ, Hudson PM, Sobotka TJ, Hong JS, Tilson HA. Extracellular concentrations of amino acid transmitters in ventral hippocampus during and after the development of kindling. *Brain Res*. 1991;540(1-2):315-318. doi:10.1016/0006-8993(91)90527-3

57. Sutherland ML, Delaney T, Noebels JL. Subtype specific down-regulation of glutamate transporter gene expression in three models of temporal lobe epilepsy. *Epilepsia*. 1997;38(5).

58. Crino PB, Jin H, Shumate MD, Robinson MB, Coulter DA, Brooks-Kayal AR. Increased expression of the neuronal glutamate transporter (EAAT3/EAAC1) in hippocampal and neocortical epilepsy. *Epilepsia*. 2002;43(3):211-218. doi:10.1046/j.1528-1157.2002.35001.x

59. Narasimhan S, Kundassery KB, Gupta K, et al. Seizure-onset regions demonstrate high inward directed connectivity during resting-state: An SEEG study in focal epilepsy. *Epilepsia*. 2020;61(11):2534-2544. doi:10.1111/epi.16686

bioRxiv preprint doi: https://doi.org/10.1101/2021.10.15.464594; this version posted October 18, 2021. The copyright holder for this preprint (which was not certified by peer review) is the author/funder. All rights reserved. No reuse allowed without permission.

60. Gupta K, Grover P, Abel TJ. Current Conceptual Understanding of the Epileptogenic Network From Stereoelectroencephalography-Based Connectivity Inferences. *Front Neurol*. 2020;0. doi:10.3389/fneur.2020.569699

61. Korzeniewska A, Cervenka MC, Jouny CC, et al. Ictal propagation of high frequency activity is recapitulated in interictal recordings: Effective connectivity of epileptogenic networks recorded with intracranial EEG. *NeuroImage*. 2014;101:96-113. doi:10.1016/j.neuroimage.2014.06.078

62. Bandt SK, Bundy DT, Hawasli AH, et al. The role of resting state networks in focal neocortical seizures. *PloS One*. 2014;9(9):e107401. doi:10.1371/journal.pone.0107401

63. Kini LG, Bernabei JM, Mikhail F, et al. Virtual resection predicts surgical outcome for drug-resistant epilepsy. *Brain J Neurol*. 2019;142(12):3892-3905. doi:10.1093/brain/awz303

64. Engel J. *Seizures and Epilepsy*. 2nd ed. Oxford University Press USA; 2013.

65. Li A, Gunnarsdottir KM, Inati S, et al. Linear Time-Varying Model Characterizes Invasive EEG Signals Generated from Complex Epileptic Networks. *Conf Proc Annu Int Conf IEEE Eng Med Biol Soc IEEE Eng Med Biol Soc Annu Conf*. 2017;2017:2802-2805. doi:10.1109/EMBC.2017.8037439

66. Frauscher B, Bartolomei F, Kobayashi K, et al. High-frequency oscillations: The state of clinical research. *Epilepsia*. 2017;58(8):1316-1329. doi:10.1111/epi.13829

67. Bragin A, Engel J, Staba RJ. High-frequency oscillations in epileptic brain. *Curr Opin Neurol*. 2010;23(2):151-156. doi:10.1097/WCO.0b013e3283373ac8

68. Staba RJ, Wilson CL, Bragin A, Fried I. Quantitative analysis of high-frequency oscillations (80-500 Hz) recorded in human epileptic hippocampus and entorhinal cortex. *J Neurophysiol*. 2002;88(4):1743-1752. doi:10.1152/jn.2002.88.4.1743

69. Jacobs J, LeVan P, Chander R, Hall J, Dubeau F, Gotman J. Interictal high-frequency oscillations (80-500 Hz) are an indicator of seizure onset areas independent of spikes in the human epileptic brain. *Epilepsia*. 2008;49(11):1893-1907. doi:10.1111/j.1528-1167.2008.01656.x

70. Fedele T, van 't Klooster M, Burnos S, et al. Automatic detection of high frequency oscillations during epilepsy surgery predicts seizure outcome. *Clin Neurophysiol*. 2016;127(9):3066-3074. doi:10.1016/j.clinph.2016.06.009

71. Jacobs J, Zijlmans M, Zelmann R, et al. High-frequency electroencephalographic oscillations correlate with outcome of epilepsy surgery. *Ann Neurol*. 2010;67(2):209-220. doi:10.1002/ana.21847

72. Papadelis C, Tamilia E, Stufflebeam S, et al. Interictal High Frequency Oscillations Detected with Simultaneous Magnetoencephalography and Electroencephalography as Biomarker of Pediatric Epilepsy. *JoVE J Vis Exp*. 2016;(118):e54883. doi:10.3791/54883

bioRxiv preprint doi: https://doi.org/10.1101/2021.10.15.464594; this version posted October 18, 2021. The copyright holder for this preprint (which was not certified by peer review) is the author/funder. All rights reserved. No reuse allowed without permission.

73. Bergey GK, Morrell MJ, Mizrahi EM, et al. Long-term treatment with responsive brain stimulation in adults with refractory partial seizures. *Neurology*. 2015;84(8):810-817. doi:10.1212/WNL.0000000000001280

74. Skarpaas TL, Jarosiewicz B, Morrell MJ. Brain-responsive neurostimulation for epilepsy (RNS® System). *Epilepsy Res*. 2019;153:68-70. doi:10.1016/j.eplepsyres.2019.02.003

75. Hartshorn A, Jobst B. Responsive brain stimulation in epilepsy. *Ther Adv Chronic Dis*. 2018;9(7):135-142. doi:10.1177/2040622318774173

76. Medvedev AV, Murro AM, Meador KJ. Abnormal interictal gamma activity may manifest a seizure onset zone in temporal lobe epilepsy. *Int J Neural Syst*. 2011;21(02):103-114. doi:10.1142/S0129065711002699

77. Guggisberg AG, Kirsch HE, Mantle MM, Barbaro NM, Nagarajan SS. Fast oscillations associated with interictal spikes localize the epileptogenic zone in patients with partial epilepsy. *NeuroImage*. 2008;39(2):661-668. doi:10.1016/j.neuroimage.2007.09.036

78. Chen D, Wan S, Bao FS. Epileptic Focus Localization Using Discrete Wavelet Transform Based on Interictal Intracranial EEG. *IEEE Trans Neural Syst Rehabil Eng*. 2017;25(5):413-425. doi:10.1109/TNSRE.2016.2604393

79. Samuel P. Burns, Sabato Santaniello, Robert B. Yaffe, et al. Network dynamics of the brain and influence of the epileptic seizure onset zone. *Proc Natl Acad Sci*. 2014;111(49):E5321-E5330.

80. Yaffe RB, Borger P, Megevand P, et al. Physiology of functional and effective networks in epilepsy. *Clin Neurophysiol Off J Int Fed Clin Neurophysiol*. 2015;126(2):227-236. doi:10.1016/j.clinph.2014.09.009

81. Khambhati AN, Davis KA, Lucas TH, Litt B, Bassett DS. Virtual Cortical Resection Reveals Push-Pull Network Control Preceding Seizure Evolution. *Neuron*. 2016;91(5):1170-1182. doi:10.1016/j.neuron.2016.07.039

82. Zijlmans M, Jiruska P, Zelmann R, Leijten FSS, Jefferys JGR, Gotman J. High-Frequency Oscillations as a New Biomarker in Epilepsy. *Ann Neurol*. 2012;71(2):169-178. doi:10.1002/ana.22548

83. Jacobs J, Zijlmans M, Zelmann R, et al. High-frequency electroencephalographic oscillations correlate with outcome of epilepsy surgery. *Ann Neurol*. 2010;67(2):209-220. doi:10.1002/ana.21847

84. Jacobs J, Wu JY, Perucca P, et al. Removing high-frequency oscillations: A prospective multicenter study on seizure outcome. *Neurology*. 2018;91(11):e1040-e1052. doi:10.1212/WNL.0000000000006158

85. Höller Y, Kutil R, Klaffenböck L, et al. High-frequency oscillations in epilepsy and surgical outcome. A meta-analysis. *Front Hum Neurosci*. 2015;9:574. doi:10.3389/fnhum.2015.00574

bioRxiv preprint doi: https://doi.org/10.1101/2021.10.15.464594; this version posted October 18, 2021. The copyright holder for this preprint (which was not certified by peer review) is the author/funder. All rights reserved. No reuse allowed without permission.

86. Wang S, So NK, Jin B, et al. Interictal ripples nested in epileptiform discharge help to identify the epileptogenic zone in neocortical epilepsy. *Clin Neurophysiol*. 2017;128(6):945-951. doi:10.1016/j.clinph.2017.03.033

87. Sindhu KR, Staba R, Lopour BA. Trends in the use of automated algorithms for the detection of high-frequency oscillations associated with human epilepsy. *Epilepsia*. 2020;61(8):1553-1569. doi:10.1111/epi.16622

88. van 't Klooster MA, van Klink NEC, Zweiphenning WJEM, et al. Tailoring epilepsy surgery with fast ripples in the intraoperative electrocorticogram. *Ann Neurol*. 2017;81(5):664-676. doi:10.1002/ana.24928

89. Worrell G, Gotman J. High-frequency oscillations and other electrophysiological biomarkers of epilepsy: clinical studies. *Biomark Med*. 2011;5(5):557-566. doi:10.2217/bmm.11.74

90. Thomschewski A, Hincapié A-S, Frauscher B. Localization of the Epileptogenic Zone Using High Frequency Oscillations. *Front Neurol*. 2019;10:94. doi:10.3389/fneur.2019.00094

91. Fisher RS, Webber WR, Lesser RP, Arroyo S, Uematsu S. High-frequency EEG activity at the start of seizures. *J Clin Neurophysiol Off Publ Am Electroencephalogr Soc*. 1992;9(3):441-448. doi:10.1097/00004691-199207010-00012

92. Jacobs J, Staba R, Asano E, et al. High-frequency oscillations (HFOs) in clinical epilepsy. *Prog Neurobiol*. 2012;98(3):302-315. doi:10.1016/j.pneurobio.2012.03.001

93. Haegelen C, Perucca P, Châtillon C-E, et al. High-frequency oscillations, extent of surgical resection, and surgical outcome in drug-resistant focal epilepsy. *Epilepsia*. 2013;54(5):848-857. doi:10.1111/epi.12075

94. Cho JR, Koo DL, Joo EY, et al. Resection of individually identified high-rate high-frequency oscillations region is associated with favorable outcome in neocortical epilepsy. *Epilepsia*. 2014;55(11):1872-1883. doi:10.1111/epi.12808

95. Liu C, Zhang R, Zhang G, et al. High frequency oscillations for lateralizing suspected bitemporal epilepsy. *Epilepsy Res*. 2016;127:233-240. doi:10.1016/j.eplepsyres.2016.09.006

96. Grinenko O, Li J, Mosher JC, et al. A fingerprint of the epileptogenic zone in human epilepsies. *Brain J Neurol*. 2018;141(1):117-131. doi:10.1093/brain/awx306

97. Gloss D, Nevitt SJ, Staba R. The role of high-frequency oscillations in epilepsy surgery planning. *Cochrane Database Syst Rev*. 2017;2017(10):CD010235. doi:10.1002/14651858.CD010235.pub3

98. Gardner AB, Worrell GA, Marsh E, Dlugos D, Litt B. Human and Automated Detection of High-Frequency Oscillations in Clinical Intracranial EEG Recordings. *Clin Neurophysiol Off J Int Fed Clin Neurophysiol*. 2007;118(5):1134-1143. doi:10.1016/j.clinph.2006.12.019

bioRxiv preprint doi: https://doi.org/10.1101/2021.10.15.464594; this version posted October 18, 2021. The copyright holder for this preprint (which was not certified by peer review) is the author/funder. All rights reserved. No reuse allowed without permission.

99. Tommaso Fedele, Georgia Ramantani, Sergey Burnos, et al. Prediction of seizure outcome improved by fast ripples detected in low-noise intraoperative corticogram. *Clin Neurophysiol*. 2017;128(7):1220-1226.

100. Buzsáki G, Silva FL da. High frequency oscillations in the intact brain. *Prog Neurobiol*. 2012;98(3):241-249. doi:10.1016/j.pneurobio.2012.02.004

101. Halász P, Szűcs A. Chapter 1 - Introductory Considerations. In: Halász P, Szűcs A, eds. *Sleep, Epilepsies, and Cognitive Impairment*. Academic Press; 2018:1-27. doi:10.1016/B978-0-12-812579-3.00001-7

102. Andrew Matsumoto, Benjamin H Brinkmann, S Matthew Stead, et al. Pathological and physiological high-frequency oscillations in focal human epilepsy. *J Neurophysiol*. 213AD;110(8):1958-1964.

103. Alkawadri R, Gaspard N, Goncharova II, et al. The spatial and signal characteristics of physiologic high frequency oscillations. *Epilepsia*. 2014;55(12):1986-1995. doi:10.1111/epi.12851

104. Engel J, da Silva FL. High-frequency oscillations - where we are and where we need to go. *Prog Neurobiol*. 2012;98(3):316-318. doi:10.1016/j.pneurobio.2012.02.001

105. Staba RJ. Normal and Pathologic High-Frequency Oscillations. In: Noebels JL, Avoli M, Rogawski MA, Olsen RW, Delgado-Escueta AV, eds. *Jasper's Basic Mechanisms of the Epilepsies*. 4th ed. National Center for Biotechnology Information (US); 2012. Accessed August 26, 2021. http://www.ncbi.nlm.nih.gov/books/NBK98191/

106. Kobayashi K, Akiyama T, Agari T, et al. Significance of High-frequency Electrical Brain Activity. *Acta Med Okayama*. 2017;71(3):191-200. doi:10.18926/AMO/55201

107. van 't Klooster MA, van Klink NEC, van Blooijs D, et al. Evoked versus spontaneous high frequency oscillations in the chronic electrocorticogram in focal epilepsy. *Clin Neurophysiol Off J Int Fed Clin Neurophysiol*. 2017;128(5):858-866. doi:10.1016/j.clinph.2017.01.017

108. Lachaux JP, Rudrauf D, Kahane P. Intracranial EEG and human brain mapping. *J Physiol-Paris*. 2003;97(4):613-628. doi:10.1016/j.jphysparis.2004.01.018

109. Logothetis NK, Pauls J, Augath M, Trinath T, Oeltermann A. Neurophysiological investigation of the basis of the fMRI signal. *Nature*. 2001;412(6843):150-157. doi:10.1038/35084005

110. Hays MA, Coogan C, Crone NE, Kang JY. Graph theoretical analysis of evoked potentials shows network influence of epileptogenic mesial temporal region. *Hum Brain Mapp*. 2021;42(13):4173-4186. doi:10.1002/hbm.25418

111. J J Maller, T Welton, M Middione, F M Callaghan, J V Rosenfeld, S M Grieve. Revealing the Hippocampal Connectome through Super-Resolution 1150-Direction Diffusion MRI. *Sci Rep*. 2019;9:2418.

bioRxiv preprint doi: https://doi.org/10.1101/2021.10.15.464594; this version posted October 18, 2021. The copyright holder for this preprint (which was not certified by peer review) is the author/funder. All rights reserved. No reuse allowed without permission.

112. Isokawa-Akesson M, Wilson CL, Babb TL. Inhibition in synchronously firing human hippocampal neurons. *Epilepsy Res*. 1989;3(3):236-247. doi:10.1016/0920-1211(89)90030-2

113. Haneef Z, Lenartowicz A, Yeh HJ, Harvey S Levin, Engel Jr J, John M Stern. Functional Connectivity of Hippocampal Networks in Temporal Lobe Epilepsy. *Epilepsia*. 2014;55(1):137-145.

114. Gaelle Bettus, Eric Guedj, Florian Joyeux, et al. Decreased basal fMRI functional connectivity in epileptogenic networks and contralateral compensatory mechanisms. *Hum Brain Mapp*. 2009;30(5):1580-1591.

115. Holmes M, Folley BS, Sonmezturk HH, et al. Resting state functional connectivity of the hippocampus associated with neurocognitive function in left temporal lobe epilepsy. *Hum Brain Mapp*. 2014;35(3):735-744. doi:10.1002/hbm.22210

116. Pereira FR, Alessio A, Sercheli MS, et al. Asymmetrical hippocampal connectivity in mesial temporal lobe epilepsy: evidence from resting state fMRI. *BMC Neurosci*. 2010;11(1):66. doi:10.1186/1471-2202-11-66